Microfluidic-assisted electrospinning, an alternative to coaxial, as a controlled dual drug release system to treat inflammatory arthritic diseases

Filipa Vasconcelos [a,b], Ana C. Lima [a,b], Walter Bonani [c,d], Catarina S. Silva [a,b], Rui L. Reis [a,b], Antonella Motta [c,d], Claudio Migliaresi [c,d], Albino Martins [a,b], Nuno M. Neves [a,b,*]

[a] 3B's Research Group, I3Bs – Research Institute on Biomaterials, Biodegradables and Biomimetics, University of Minho, Headquarters of the European Institute of Excellence on Tissue Engineering and Regenerative Medicine, AvePark, Parque de Ciência e Tecnologia, Zona Industrial da Gandra, 4805-017 Barco, Guimarães, Portugal

[b] ICVS/3B's - PT Government Associate Laboratory, Braga/Guimarães, Portugal

[c] Department of Industrial Engineering, University of Trento, Via Sommarive 9, 38123 Trento, Italy

[d] BIOtech Research Centre, University of Trento, Via delle Regole 101, 38123 Trento, Italy

ABSTRACT

Inflammatory arthritic diseases are characterized by a persistent inflammation of the synovial tissues where tumor necrosis factor alpha (TNFα) and interleukin-6 (IL-6) pro-inflammatory cytokines are over-expressed, leading to progressive musculoskeletal disability. Methotrexate (MTX), a disease-modifying-anti-rheumatic drug (DMARD) commonly applied in their treatment, can be used in combination with biological-DMARDs as anti-TNFα antibody to improve the treatments efficacy. However, their systemic administration comes with severe side-effects and limited therapeutic efficacy due to their off-target distribution and short half-life. To overcome such limitations, encapsulation of clinically relevant concentrations of MTX and anti-TNFα antibody into polycaprolactone (PCL) or poly(vinyl-alcohol) (PVA) microfluidic-assisted or coaxial electrospun fibrous meshes is proposed as local controlled dual drug release systems.

Release studies show that microfluidic-assisted electrospinning meshes encapsulating both drugs achieved higher concentrations than coaxials. Biological assays using human articular chondrocytes (hACs) and monocytic cells (THP-1 cell line) demonstrate that fibrous meshes encapsulating the drugs are non-toxic. The systems' efficacy is proved by a significant decrease of TNFα and IL-6 concentrations in conditioned medium of lipopolysaccharide (LPS)-stimulated THP-1 cells, especially in the presence of microfluidic-assisted electrospun meshes, when compared with THP-1 conditioned medium (59.5% and 83.9% less, respectively).

Therefore, microfluidic-assisted electrospinning fibrous meshes with encapsulating drugs represent an alternative to coaxial, as a local therapy for inflammatory arthritis diseases.

1. Introduction

Inflammatory arthritic diseases, namely rheumatoid arthritis (RA) and osteoarthritis (OA), are associated with progressive disability due to a persistent inflammation in the synovial tissues that may affect multiple or isolated joints of the human body, respectively. Furthermore, a persistent synovial inflammation leads to erosive joint damage and functional impairment of thousands of people worldwide, especially in the elderly. Clinical manifestations involve arthralgia, swelling, redness, destruction of the bone and cartilage joints, weakness of the tendons and ligaments, pain, mobility limitations and musculoskeletal disability [1].

Currently, the available therapeutic treatments aim to reduce the diseases' activity or even reach a clinical remission state. Pharmacological therapies comprise non-steroidal anti-inflammatory drugs (NSAIDs), which can reduce the pain and stiffness or even improve the physical function by reducing inflammation, but they don't have protective effects in damaged joints [2]. By its side, glucocorticoids offer rapid symptomatic and disease-modifying effects but are associated with serious long-term side-effects and do not hinder disease progression, as reviewed elsewhere [3]. Disease modifying anti-rheumatic drugs

---

(DMARDs) are used as gold-standard treatment since they can target inflammation and reduce structural damage. It has been achieved significant progress towards disease remission without joint deformity in patients treated with DMARDs [4], namely when using Methotrexate (MTX) as the first-line treatment [5]. In combination with biological DMARDs such as tumor necrosis factor (TNF) inhibitors (for example: Infliximab, Adalimumab, Certolizumab pegol, Etanercept and Golimumab); interleukin-6 (IL-6) receptor inhibitior (Tocilizumab), T-cell blockage or B-cell depletion (Rituximab and Ofatumumab), the treatment efficacy can be improved [6].

Several drug delivery systems (DDS) were been developed [7], aspiring the control of the drug release kinetics by playing with specific parameters such as polymer type, molecular weight, or processing method [8]. More specifically, intra-articular (IA) injection of DDS allow the release of a drug in the targeted area, decreasing both the off-targeting distribution and the amount of required drug, thus avoiding systemic side effects [9,10]. Novel strategies such as polymeric micro-[11] or nano-particles [12] are in development for *in situ* drug release. Indeed, bioactive molecules and drugs can be loaded and delivered by microparticles [13].

Electrospun fibrous meshes were also been explored as drug carriers mainly due to their high surface area,and the fast and efficient solvent evaporation during processing, which limited the recrystallization of incorporated drug, favoring the formation of amorphous dispersions, as reviewed elsewhere [14]. Despite the advancements on the use of electrospun fibrous meshes as DDS, the initial burst release remains unavoidable, making them not ideal for a sustained drug release. To surpass this limitation, several complex post-processing treatments can be applied such as cross-linking or chemical modifications. These treatments, however, may lead to toxicity and to a reduction in biocompatibility. Several modifications were made to the conventional electrospinning set-up, enabling the production of meshes with enhanced performancesuch as core-shell fiber meshes produced through coaxial electrospinning, in which the nanofiber core polymer is surrounded by a layer of another polymer (shell) [15]. With this technique it is possible to simultaneously encapsulate two different drugs and/or growth factors, one in the shell and another in the core of the fibers [16,17], obtaining dual drug delivery systems [18,19]. The use of co-axial electrospinning offers several advantages as a DDS such as: (i) the coating effect of the fibers' shell that can protects the inner compounds from premature degradation; (ii) the specific core-shell structure that facilitates the incorporation of active drugs in the core; (iii) can prevents the burst or premature release; (iv) enables a sustained release for a longer periods; (v) enhances the therapeutic efficacy and reduces toxicity and; (vi) can protects the drugs from potential damage caused by any post-processing treatment, as reviewed elsewhere recently [20].

Conversely, microfluidic devices allow setting a controlled and reproducible flow of different and separate polymeric solutions [21,22]. Microfluidic devices have been used in combination with micro-fabrication techniques to create DDS that combine different materials with the purpose of deliver two or more drugs [23]. However, those systems are macroscopic, difficult to downsize, and most of the times used with water-based solutions to create hydrated hydrogel constructs (with consequent limitations in terms of delivery kinetics, long-term stability and availability of the drugs), as reviewed elsewhere [24].

Although the previously mentioned techniques can provide platforms to produce combined therapeutic materials, their principle is similarly based on multiple-chamber and extremely complex set-up structures. Currently, no reports were found using single chamber platforms for the development of combined therapeutic materials/fibers. As such, to fill out this gap, a novel methodology named microfluidic-assisted electrospinning will be herein implemented and optimized. This technique allows the creation of nanofibers with variable composition prepared from two different polymeric solutions in a continuous exchanging way, each carrying a different drug. This methodology will take advantage of the major characteristics of each

technique and try to surpass the limitations of both. The microfluidic system will contribute with a high degree of control over flow of the polymeric solutions and the high reproducibility [21,22]. The integration of the microfluidic system in the electrospinning setup will allow a faster solidification of the solutions and the downsizing of the fibers, enabling to create fibrous meshes from two distinct polymers [25].

We prepared and characterized a controlled dual drug release system by encapsulating MTX and anti-TNFα antibody into polycaprolactone (PCL) and poly(vinyl-alcohol) (PVA) fibers, respectively, produced by microfluidic-assisted electrospinning. For comparison, both drugs were also encapsulated into coaxial fibers processed by coaxial electrospinning, consisting of a PCL shell loaded with MTX and a PVA core loaded with the antibody. Parameter optimization and characterization of the coaxial and microfluidic-assisted electrospinning fibrous meshes, as well as the release profile of encapsulated pharmaceutical agents (i.e., MTX and anti-TNFα) was determined. Furthermore, the *in vitro* safety and efficacy of the developed controlled release systems were evaluated with human articular chondrocytes (hACs) and monocytic cells (THP-1 cell line).

2. Materials and methods

2.1. Materials

Polycaprolactone (PCL; average Mn 80000), poly(vinyl alcohol) (PVA; average Mw 85,000–124,000, 87–89% hydrolyzed), fluorescein 5 (6)-isothiocyanate (FITC), rhodamine B (RhB) isothiocyanate, methotrexate (MTX; meets USP testing specifications), papain, N-acetyl cysteine, chondroitin sulphate and EDTA were purchased from Sigma-Aldrich (Saint Louis, MO, USA). PCL and PVA were kept at room temperature, fluorescein and RhB were kept in the dark, and MTX was stored at −20 °C. Chloroform (CHCl$_3$) and N-N-Dimethylformammide (DMF) were purchased from Honeywell (Germany) and kept at room temperature. Anti-TNFα antibody was purchased from Abcam (Cambridge, UK) and stored at −20 °C. Human TNFα and Human IL-6 Duo Set ELISA Kits were purchased from R&D Systems (Minneapolis, MN, USA) and stored at 4 °C.

2.2. Production of fibrous meshes

2.2.1. Solutions preparation

A 10% (w/v) solution was prepared by dissolving PCL in CHCl$_3$ and DMF (4:1) and stirred until complete dissolution. A 8% (w/v) solution was prepared by dissolving PVA in water. For fluorescence microscopy analysis, 3 mg of FITC was added directly to the 10% (w/v) PCL solution and 3 mg of RhB to the 8% (w/v) PVA solution. For the encapsulating drugs, the pharmaceutical agents were defined according to the dose that is clinically approved for use in the treatment of inflammatory arthritic diseases. Therefore, a given amount of MTX powder was added to the PCL solution to obtain a 25 μg mL^{-1} of MTX solution in the given solvent [1], and anti-TNFα antibody was added to the PVA solution to obtain a 5 μg mL^{-1} solution [26]. All the solutions were kept under constantly stirring to avoid phase separation, and the solutions with the dyes were kept in the dark.

2.2.2. Conventional and coaxial electrospinning

For the conventional electrospinning processes, syringes of 6 mL (Braun, Germany) were filled with the polymeric solutions and connected to a blunted metallic 21 G needle. For the coaxial electro-spinning, a coaxial needle (Holmarc Opto-Mechatronics, India) was used to allow the simultaneous flow of the two different polymeric solutions, leading to the production of core/shell or hollow fibers. Those optimized parameters (displayed on Tables 1a and 1b) were also applied to electrospin the solutions containing the fluorescent dyes or the drugs. It is important to underline that distinct collecting times were settled aiming to obtain equivalent quantities of each polymer in the different fibrous

Table 1a

Optimized conventional electrospinning parameters.

Solution	Flow rate [mL h^{-1}]	Applied voltage [kV]	Needle to collector distance [cm]	Collecting time [h]	Temperature [°C]	Relative humidity [%]
PCL	0.7	15	20	1.4	22 ± 2	35
PVA	0.5	18		2		42

Table 1b

Optimized coaxial electrospinning parameters.

Solution	Flow rate [mL h^{-1}]	Applied voltage [kV]	Needle to collector distance [cm]	Collecting time [h]	Temperature [°C]	Relative humidity [%]
PCL (shell)	0.7	15	20	1.4	22 ± 2	35
PVA (core)	0.5	18		2		42
PCL + PVA (full coaxial)	0.7 (shell) 0.5 (core)	16		1.7		40

meshes. The fibrous meshes were extracted from the planar collector and cut for further assays.

2.2.3. Microfluidic-assisted electrospinning

The microfluidic system was composed of a controllable microfluidic 2/3 port solenoid valve (Elveflow, France) with two available channels; a microfluidic valve controller (MUX wire and ESI software from Elveflow, France); and a pressure system at 1–3 bar with a pressure controller (Fisnar, USA). The PCL solution was loaded into a 10 mL syringe connected to the channel 1 (CH$_1$) of the solenoid valve, whereas the PVA solution entered channel 2 (CH$_2$). A 10 cm PTFE tube connected to the exit of the solenoid valve was inserted into a blunted metallic needle (21 G), which was further connected to the high voltage power supply of the electrospinning setup (Fig. 1).

The PCL or PVA solutions were first tested separately to serve as experimental controls, leaving either CH1 or CH2 continuously open. To create a solution with both polymers, the commuting time between both channels of the solenoid valve was optimized. It is important to underline that until similar lengths (≈1 cm) of each polymeric solution in the PTFE tubes were achieved, without mixing or clogging the tubes, by actively modifying the frequency of the solenoid valve, the electrospinning component was not added to the microfluidic system.

Those optimized parameters (displayed on Table 2) were also applied to electrospin the solutions containing the fluorescent dyes or the drugs. It is important to underline that distinct collecting times were settled aiming to obtain equivalent quantities of each polymer in the different fibrous meshes. The fibrous meshes were extracted from the planar collector and cut for further assays.
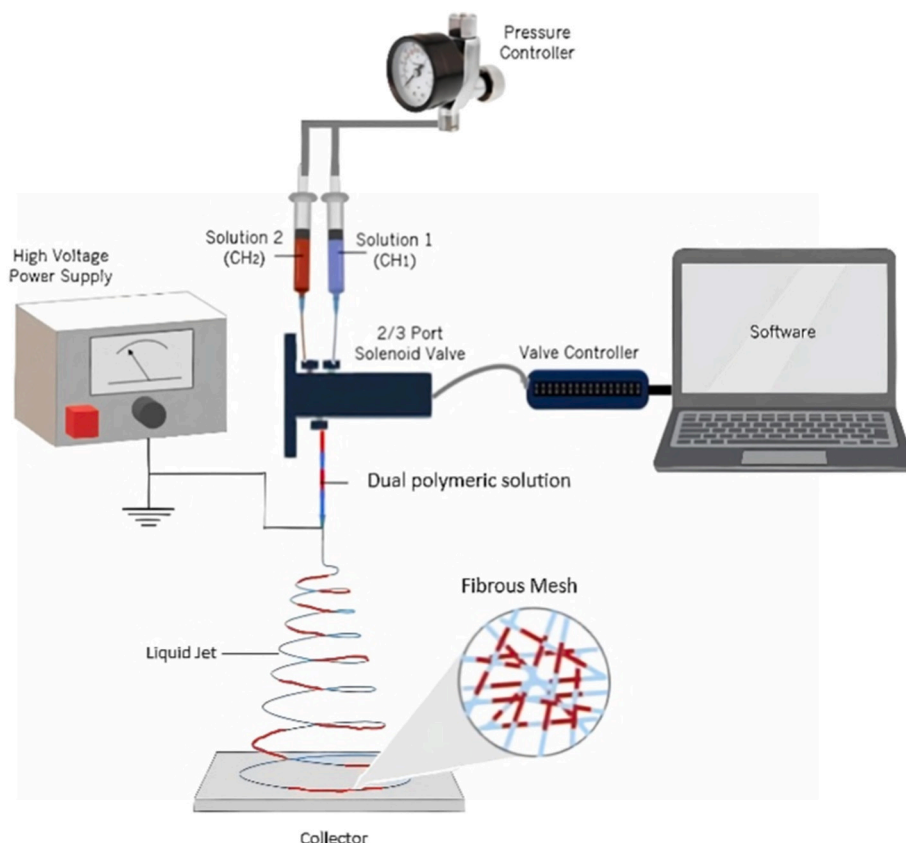
Fig. 1. Schematic representation of a microfluidic-assisted electrospinning set-up.

Table 2
Optimized microfluidic-assisted electrospinning parameters.

Solution	Microchannel opening [s]	Pressure [bar]	Applied voltage [kV]	Needle to collector distance [cm]	Collecting time [h]	Temperature [°C]	Relative humidity [%]
PCL (CH$_1$)	Always open	1.5	16	20	1.4	22 ± 2	38
PVA (CH$_2$)	Always open	3	18		2		43
PCL + PVA	1.5 (CH$_1$) 0.5 (CH$_2$)	2	17		3.5		41

2.3. Characterization of the fiber meshes

2.3.1. Fluorescence microscopy

To verify the distribution of the fluorescently labelled polymeric solutions on a fibrous mesh, 10 samples of each electrospun condition were collected on glass slides during 5 s. The samples were analyzed in a Transmitted and Fluorescence Light Microscope (model Axio Imager Z1m; Zeiss, Germany), taken at 20× magnifications, and the images were treated with ZEN – Digital Imaging for Light Microscopy software (Zeiss, Germany). Excitation wavelengths were 490 nm for FITC and 553 nm for RhB.

2.3.2. Scanning electron microscopy

The electrospun samples were sputter-coated with gold (coater 108 A; Cressington, United States) for 2 min at 15 mA and, then, analyzed by scanning electron microscope (SEM; JSM-6010 LV model; JEOL, Japan), with an acceleration voltage of 5–10 kV, and taken at the magnification of 2000×. At least 7 micrographs of each condition were used to assess the fibrs' diamater. This analysis was performed with *DiameterJ* plugin created for *ImageJ* (National Institute of Health, USA).

2.3.3. Differential scanning calorimetry

Differential Scanning Calorimetry (DSC) was used to determine the thermal properties (i.e., melting temperature (T_m), crystallization temperature (T_c), melting enthalpy (ΔH_m), crystallization enthalpy (ΔH_C)) of the different fibrous meshes. For PCL or PVA processed by conventional, coaxial, or microfluidic-assisted electrospinning, PCL + PVA and PCL after PVA leaching processed by coaxial or microfluidic-assisted electrospinning, 5 independent samples were weighed (3.88±0.23 mg each), packed into aluminum pans, and then analyzed by DSC (DSC Q100 model; T.A. Instruments, USA), with one heating and cooling cycle. For the calibration of the equipment, 3.88 mg of Indium was used, and all the experiments were conducted under a nitrogen atmosphere (flow rate 50 M min^{-1}). The calorimetric measurements were recorded between 0 °C and 100 °C (PCL), or 220 °C (for PVA, PCL + PVA) at a heating rate of 10 °C/min, and then cooled down to 0 °C, at the same temperature rate.

2.3.4. Uniaxial tensile tests

Fibrous mesh strips of 18 mm × 5 mm were fixed in paper frames with a testing area of 10 mm × 10 mm. The thickness (0.5 ± 0.08 mm) of the samples was measured using a digital micrometer (Mitutoyo, Japan). 6 independent samples, in triplicate, of PCL or PVA processed by conventional, coaxial, or microfluidic-assisted electrospinning, PCL + PVA and PCL after PVA leaching prepared by coaxial or microfluidic-assisted electrospinning were tested under dry conditions, at room temperature. Right before the mechanical test, the lateral sides of the paper frames were cut. Uniaxial tensile properties were measured using a universal mechanical testing equipment (model 5543; INSTRON, UK), equipped with a 50 N load cell. A crosshead speed of 2 mm min^{-1} and a 10 mm gauge length were used. The mechanical tests were performed until complete fracture of the samples. Load and displacement measurements were acquired, and the tensile stresses and strains were calculated from the raw data. A linear regression of the maximum slope at linear region from stress-strain curves was used to calculate the Elastic Modulus.

2.4. Drug release profiles

Fibrous meshes (10 mm × 10 mm, *n = 3*) of each electrospinning processing condition were immersed in 10 mL of PBS, kept in a water bath at 37 °C and under an agitation of 60 rpm. The release study was conducted for 11 days, corresponding approximately to the half-life of anti-TNFα antibody in circulation [27]. Sampling was performed at each time point (0, 0.5, 1, 2, 3, 4, 6, 8, 10, 12, 24, 36, 48, 60, 72, 84, 96, 108, 120, 168, 216 h) by taking 1 mL of the releasing solution from each condition and adding 1 mL of fresh PBS and stored at −20 °C until further analysis.

2.4.1. Quantification of released methotrexate

For tracing the MTX release profile, the following fibrous meshes were tested: PCL, PCL + PVA, PCL with encapsulated MTX, and PCL + PVA with encapsulated MTX processed either by coaxial or microfluidic-assisted electrospinning. The release study was conducted as described previously. Standards of MTX were performed ranging from 0 to 25 µg mL^{-1}. Then, 150 µL of samples or standards in triplicate were added to each 96 well quartz plate. The absorbance was measured using a microplate reader (model Synergy HT; BioTek Instruments, USA) at 303 nm. The release of MTX for each sample was calculated from the standard curve.

2.4.2. Quantification of released anti-TNFα antibody

For tracing the anti-TNFα antibody release profile, the following fibrous meshes were tested: microfluidic-assisted electrospinning of PVA and PCL + PVA fibrous meshes, and coaxial electrospinning or microfluidic-assisted electrospinning of PVA with encapsulated anti-TNFα antibody, and PCL + PVA with encapsulated anti-TNFα antibody. The release study was conducted as described previously. The released anti-TNFα antibody was quantified by the MicroBCA™ Protein Assay Kit (Pierce, ThermoFisher Scientific; Rockford, IL, USA), according to the manufacturer's instructions. A set of BSA standards were prepared in PBS at concentrations ranging from 0 to 40 µg mL^{-1}. 150 µL of both samples and standards were added to each 96 well plate, in triplicate. The plates were covered to protect it from light exposure and incubated at 37 °C for 2 h. After, the plates were cooled to room temperature and the absorbance at 562 nm was measured in a microplate reader (model Synergy HT; BioTek Instruments, USA). The released anti-TNFα antibody concentration was calculated from the protein standard curve.

2.5. Biological assays

2.5.1. Cells isolation and expansion

To evaluate cytotoxicity of the processed fibrous meshes, human articular chondrocytes (hACs) were isolated from knee cartilage samples collected from arthroplasties surgeries biopsies. These samples were obtained under the cooperation agreement established between the Centro Hospitalar do Alto Ave, Guimarães, Portugal, and the 3B's Research Group, after obtaining informed donor consent. Cells were isolated by enzymatic digestion, according to a previously described protocol [28]. hACs cells were cultured in Dulbecco's modified Eagle's medium (DMEM, Sigma Aldrich, USA), supplemented with 10% fetal bovine serum (FBS), 10 mM HEPES buffer (Life Technologies, Paisley,

UK), L-lanyl-ʟ-glutamine (Sigma Aldrich, USA), MEM non-essential amino acids (Sigma Aldrich, USA): 100 units mL^{-1} of penicillin, 100 µg mL^{-1} of streptomycin, and 10 ng mL^{-1} human basic fibroblast growth factor (bFGF). Cells in culture were incubated at 37 °C in a humidified 5% CO_2 atmosphere. To evaluate the efficacy of the processed fibrous meshes, human monocytic cells (THP-1 cell line) was maintained in complete RPMI (cRPMI), containing RPMI 1640, supplemented with 2 mM ʟ-glutamine, 100 units mL^{-1} of penicillin, 100 µg mL^{-1} of streptomycin, 10 mM Hepes buffer and 10% FBS.

2.5.2. Cell cultures with fibrous meshes

Electrospun fibrous meshes from the different conditions were cut into 10 mm × 10 mm, placed into 24 well plates, and sterilized by UV radiation during 30 min on each side. Electrospun fibrous meshes without the pharmaceutical agents and with free drugs were used as controls. hACs were seeded at the top of each fibrous mesh at $1,50 \times 10^5$ cells/well in non-adherent plates, using the concentrated droplet method, and after 4 h of cell attachment, the culture medium was added to a final volume of 1 mL. After 1, 3, and 7 days of culture, the different samples in triplicate were washed with sterile DPBS and analyzed regarding cell viability (Alamar Blue assay), cell proliferation (DNA quantification), and total protein and glycosaminoglycan synthesis. THP-1 cell line was seeded at 5×10^5 cells/well in cRPMI with 100 nM phorbol 12-myristate-13-acetate (PMA) for 24 h. After incubation, nonattached cells were removed by aspiration, and the adherent cells were washed three times with cRPMI. To ensure reversion of cells to a resting macrophage phenotype before stimulation, cells were incubated for an additional 48 h in cRPMI without PMA. After 24 h stimulation with 100 ng/mL of lipopolysaccharide (LPS) to model inflammation *in vitro*, the different fibrous meshes were added to the cultures. Conditioned medium from all the conditions were collected, in triplicate, at the following time points: 1, 3 and 7 days. Afterwards, the different samples in triplicate were washed with sterile DPBS and analyzed regarding cell viability (Alamar Blue assay) and cell proliferation (DNA quantification).

2.5.3. Cell metabolic activity

Cell metabolic activity was evaluated by the Alamar Blue (Bio-Rad, UK) assay. The culture medium was removed, and each sample was thoroughly washed with DPBS. A solution of 1:10 Alamar blue in culture medium was added to each well/sample, as well as background samples of unseeded fibrous meshes. Samples were then incubated for 4 h at 37 °C and 5% CO_2, protected from light exposure. The fluorescence was measured in a microplate reader (model Synergy HT; Bio-Tek Instruments, USA) at the excitation and emission wavelengths of 530 and 590 nm, respectively. Background fluorescence was subtracted from the values of each sample.

2.5.4. Immunofluorescence

The morphology of hACs was analyzed by laser scanning confocal microscopy (Leica SP8, Germany). Samples were fixed in 10% formalin until further use. After washing with DPBS, samples were incubated with 10% FBS for one hour at RT, followed by an incubation with Phalloidin-Rhodamine (Sigma-Aldrich, USA) and DAPI (Biotium, USA) for twenty minutes at RT. Representative images were acquired in randomly selected locations of the cell seeded meshes.

2.5.5. Glycosaminoglycans quantification

Before the glycosaminoglycans (GAGs) quantification, the fibrous meshes seeded with hACs were collected and stored in Eppendorf tubes at −80 °C until further analysis. A digestion solution was prepared by adding papain (Sigma Aldrich, USA) and *N*-acetyl cysteine (Sigma Aldrich, USA) at concentrations of 0.05% and 0.096%, respectively, to 50 mL of digestion buffer (200 mM of phosphate buffer containing 1 mM EDTA (Sigma Aldrich, USA) with pH 6.8). Each sample was incubated overnight at 60 °C with 600 µL of digestion buffer. Then, after a 10 min

centrifugation at 13,000 rpm, the supernatants were collected. A dimethymethylene blue (DMB) stock solution was prepared by dissolving 16 mg of DMB powder in 900 mL of distilled water containing 3.04 g of glycine and 2.73 g of NaCl. pH was adjusted to 3.0 with HCl and the volume adjusted to 1 L. The solution was stored at room temperature and covered with an aluminum foil. A chondroitin sulphate (Sigma Aldrich, USA) solution was prepared in water at 5 mg mL^{-1} and kept refrigerated. Standards with concentrations ranging from 0 to 5 µg mL^{-1} were prepared from serial dilutions of the previous solution. The absorbance at 525 nm was measured in triplicate using a microplate reader (model Synergy HT; BioTek Instruments, USA). The total GAGs concentration of each sample was calculated from the standard curve.

2.5.6. Cell proliferation

Cell proliferation was quantified by the Quant-iT™ PicoGreen® dsDNA Assay Kit (Life Technologies; ThermoFisher Scientific, USA) according to manufacturer's instructions. Previously, the samples were collected at each timepoint, washed with DPBS, placed in Eppendorf tubes with 1 mL of ultrapure water, and frozen at −80 °C until further testing. Before the assay, the samples were placed into a ultrasonic water bath (model SONOREX DIGITEC DT 100 H; Bandelin, Deutchland) for 15 min. A set of DNA standards was prepared in ultrapure water at concentrations ranging from 0 to 2 µg mL^{-1}. The fluorescence of each sample was measured, in triplicates, on a white opaque 96 well plate (Costar) using an excitation wavelength of 485 nm and an emission wavelength of 528 nm, being the concentration of DNA in the samples was calculated from the standard curve.

2.5.7. Bioactivity of released anti-TNFα antibody

The amount of TNFα in the conditioned medium of THP-1 cells was assessed by ELISA, using the commercial Human TNFα Duo Set ELISA Kit (R&D Systems, USA), according to instructions of the manufacturer. Absorbance was read at 450, 540 and 570 nm on a microplate reader (model Synergy HT; BioTek Instruments, USA). A standard curve was built with concentrations ranging from 0 to 1000 pg ml^{-1}, and the concentration of TNFα calculated from the standard curve.

2.5.8. Bioactivity of released methotrexate

It is described that the treatment of inflammatory arthritic diseases with MTX reduces the concentration of several pro-inflammatory cytokines, namely IL-6 [29]. Hence, the amount of IL-6 in the conditioned medium of THP-1 cells, cultured in the presence of the different fibrous meshes, was assessed using a commercial Human IL-6 Duo Set ELISA Kit (R&D Systems; USA), according to the manufacturer instructions. Absorbance was read at 450, 540 and 570 nm on a microplate reader (model Synergy HT, BioTek Instruments, USA). A standard curve was built with concentrations ranging from 0 to 600 pg mL^{-1}, and the concentration of IL-6 calculated from the standard curve.

2.6. Statistical analysis

Statistical analysis was performed using Graph Pad PRISM version 6.01. First, a Shapiro-Wilk test was used to ascertain the data normality. For all quantitative data the normality was rejected, and non-parametric tests were used (Krustal-Wallis test followed by Dunn's test for multiple comparisons, and Mann-Whitney test to compare two conditions). P values lower than 0.05 were considered statistically significant and the results were expressed as median±interquartile range.

3. Results

3.1. Characterization of the fiber meshes

3.1.1. Fluorescence microscopy

For each sample analyzed via fluorescence microscopy, three images are displayed in Fig. 2: two of the split channels (Fluorescein – first
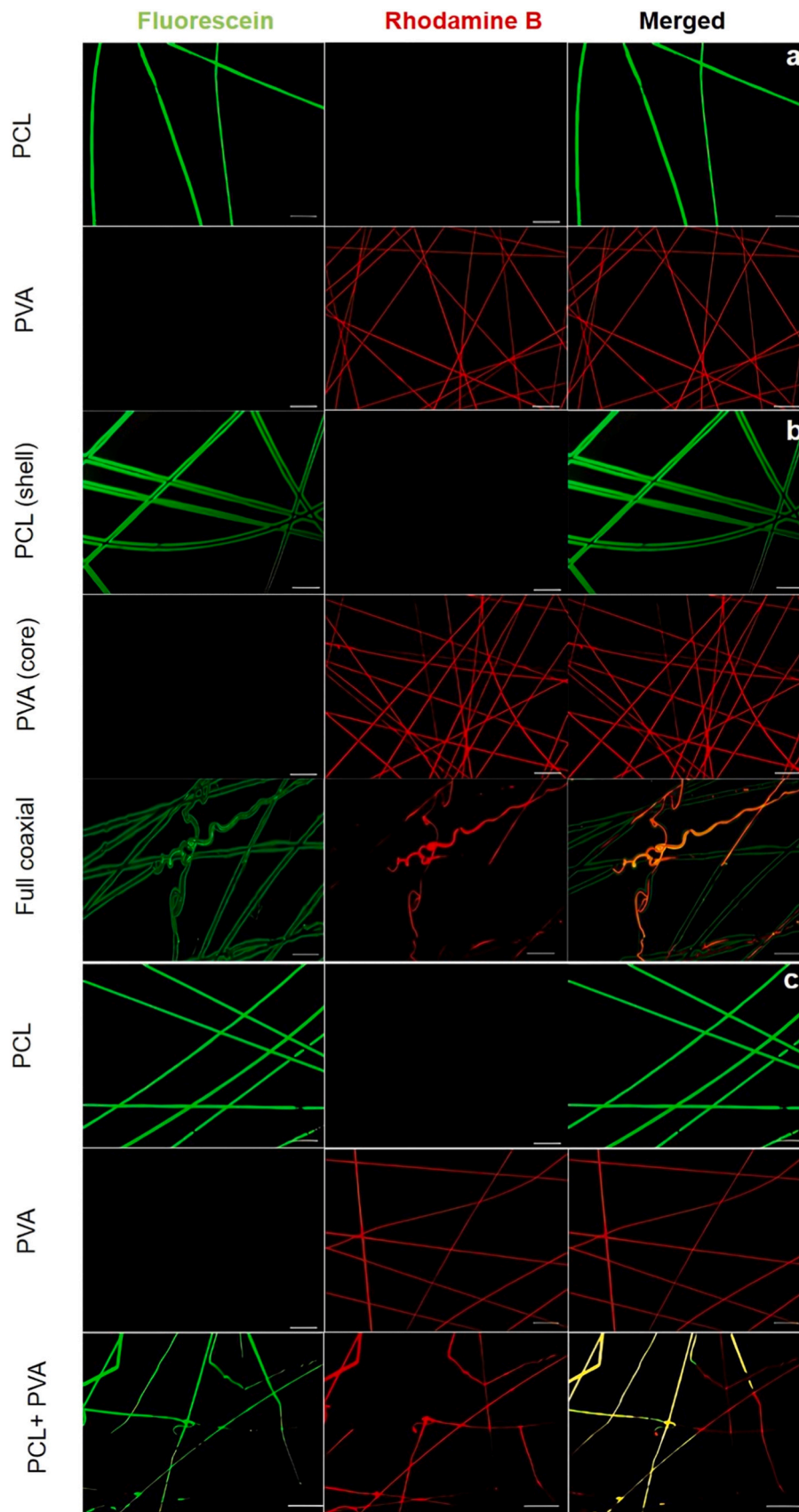
Fig. 2. Fluorescence microscopy images at 20× magnification (Fluorescein, Rhodamine B and Merged) for each condition: a) conventional electrospinning of PCL and PVA; b) coaxial electrospinning of PCL (shell), PVA (core) and full coaxial; and c) microfluidic-assisted electrospinning of PCL (CH_1), PVA (CH_2), and PCL + PVA fibers. Scale bar: 50 μm.

image, or RhB – second image) and one merged image (last image).

Regarding conventional electrospinning (Fig. 2a), only one of the fluorescent dyes is observed, and all the solutions were able to produce fibers with random orientation and no relevant defects such as beads were observed. The samples made of PCL also appear to have a higher diameter than the fibers made of PVA. Fluorescence microscopy analysis of coaxial electrospinning (Fig. 2b) demonstrated the presence of PCL fibers with a hollow structure and PVA thinner solid fibers. Moreover, the coaxial fibers have an evident core-shell structure, proving that the PVA fibers fit perfectly inside the shell made of PCL. The microfluidic-assisted electrospinning (Fig. 2c) allows to produce fibers with random orientation and without noticeable defects. The fluorescence images confirmed the presence of both polymers in the same fibrous mesh, by having the two different dyes easily distinguishable from each other. Overlapping regions are also possible to be observed (where the yellow color appears).

3.1.2. Scanning electron microscopy

Fig. 3 shows representative SEM images, as well measured fiber diameter histograms for each fibrous mesh.

In the conventional electrospinning (experiment controls) (Fig. 3a), the fibers are randomly aligned, do not have defects (absence of beads) and present a smooth surface. The diameter of the PCL fibers is 4% below 0.5 μm, 19% having diameters between 0.5 and 1 μm, 49% with diameters between 1 and 1.5 μm, and 23% with diameters higher than 1.5 μm. PVA fibers are considerably smaller than the PCL ones, being 93% of them below 0.5 μm, 6% between 0.5 and 1 μm, and 1% higher than 1 μm.

SEM micrographs of coaxial electrospinning (Fig. 3b) showed fibers similar to the ones processed by conventional electrospinning. The diameters of PCL fibers (shell) are 3% below 0.5 μm, 23% with diameters between 0.5 and 1 μm, 48% with diameters between 1 and 1.5 μm, and 26% of the diameters higher than 1.5 μm. On the other hand, the diameter of PVA fibers (core) is 79% of them below 0.5 μm, 20% with diameters between 0.5 and 1 μm, and 1% with diameters higher than 1 μm. Lastly, the diameters of full coaxial fibers are 11% below 0.5 μm, 60% having diameters between 0.5 and 1 μm, 15% between 1 and 1.5 μm, and 12% of the diameters higher than 1.5 μm.

SEM micrographs of PCL (CH_1), PVA (CH_2), and PCL + PVA fibers processed by microfluidic-assisted electrospinning (Fig. 3c) showed randomly oriented fibers and without evident defects. The diameter of the PCL fibers is 3% of them below 0.5 μm, 22% between 0.5 and 1 μm, 51% between 1 and 1.5 μm, and 24% higher than 1.5 μm. On the other hand, the diameter of the PVA fibers is 87% below 0.5 μm, 10% between 0.5 and 1 μm, and 3% higher than 1 μm. Lastly, the fibers with both polymers have 52% below 0.5 μm, 26% between 0.5 and 1 μm, 15% between 1 and 1.5 μm, and 7% higher than 1.5 μm of diameter. It is also important to notice that the fibrous meshes made of both polymers and processed by microfluidic-assisted electrospinning had two distinct populations of fibers' diameter.

3.1.3. Differential scanning calorimetry

The DSC curves are shown in Fig. 4, whereas the melting (T_m) and crystallization (T_c) peak temperatures, as well as melting (ΔH_m) and crystallization (ΔH_c) enthalpy values are represented in Table 3. It is also important to underline that this characterization test performed, mainly, to demonstrate the presence of PCL and PVA in fibrous meshes where both polymers were being electrospun. In addition, a condition where PVA fibers were leached out from coaxial or microfluidic-assisted fibrous meshes with both polymers (after 24 h immersion in water) was also tested to evaluate the thermal properties of the remaining PCL upon PVA dissolution.

DSC results shown that the fibrous meshes made of PCL had a peak (T_m) of 56.2±1.5 °C for the conventional electrospinning, 55.3±1.5 °C for the coaxial electrospinning (shell fibers), and 56.9±2.5 °C for the microfluidic-assisted electrospinning (Fig. 4a). Moreover, PCL fibrous

meshes had a peak (T_c) of 20.4±1.0 °C for the ones processed by conventional electrospinning, 21.5±0.5 °C for the coaxial electrospinning (shell fibers), and 23.6±0.9 °C for microfluidic-assisted electrospinning. By its side, the PVA fibers showed a peak (T_m) of 194.3±0.4 °C for the ones processed by conventional electrospinning, 191.1±2.9 °C for co-axial electrospinning (core fibers), and 195.1±1.8 °C for microfluidic-assisted electrospinning (Fig. 4b). PVA (87–89% hydrolyzed) also displays peaks between 58 and 67 °C, corresponding to its water content, which overlaid the glass transition temperature of the polymer.

Lastly, the fibrous meshes processed by coaxial electrospinning had two (T_m) (two easily distinguishable peaks on the curve) of 58.5±0.3 °C and 182.4±2.5 °C, corresponding to PCL and PVA, respectively, and 54.7±2.7 °C and 182.2±3.5 °C in the case of microfluidic-assisted electrospinning (Fig. 4c). Moreover, the fibrous meshes processed by coaxial electrospinning had peak (T_c) of 27.2±1.0 °C, and the ones regarding microfluidic-assisted electrospinning combining both solutions were 15.9±2.1 °C, similar to the (T_c) of PCL. Considering the envisioned biomedical application, the coaxial and microfluidic-assisted electrospinning fibrous meshes were immersed in water for 24 h, simulating the leaching of PVA from the samples. The (T_m) peaks of the fibrous meshes were 58.7±0.8 °C and 59.3±0.3 °C for coaxial and microfluidic-assisted electrospinning, respectively, and their (T_c) peaks were 33.8±1.9 °C and 22.5±1.2 °C.

Regarding the enthalpy values, the fibrous meshes made of PCL had (ΔH_m) of 28.9±1.4 J g^{-1} for the conventional electrospinning, 27.8±0.9 J g^{-1} for the coaxial electrospinning, and 17.4±0.4 J g^{-1} for the microfluidic-assisted electrospinning. Their (ΔH_c) were 25.4±1.3 J g^{-1}, 26.9±0.8 J g^{-1}, and 20.3±1.2 J g^{-1}, respectively. By its side, the PVA fibers showed (ΔH_m) of 17.8±3.5 J g^{-1} for the ones processed by conventional electrospinning, 13.4±1.5 J g^{-1} for coaxial electrospinning, 11.0±1.0 J g^{-1} and for microfluidic-assisted electrospinning. Melting enthalpy values for the fibrous meshes produced by coaxial and microfluidic-assisted electrospinning where both polymers were processed were 30.8±0.7 J g^{-1} and 26.8±1.9 J g^{-1} for the PCL; 17.2±1.4 and 15.5±3.4 J g^{-1} for the PVA, respectively. Their (ΔH_c) were 27.3±0.5 J g^{-1} and 24.3±0.2 J g^{-1} for coaxial and microfluidic-assisted electrospinning. Lastly, the coaxial and microfluidic-assisted electrospinning fibrous meshes immersed in water had (ΔH_m) of 18.3±1.4 J g^{-1} and 14.4±2.0 J g^{-1}, and (ΔH_c) of 15.6±1.3 J g^{-1} and 13.4±1.9 J g^{-1}, respectively.

3.1.4. Uniaxial tensile test

For the PCL fibrous meshes processed by the different electrospinning techniques (Fig. 5a), the stress-strain curve of coaxial electrospinning has a lower tensile stress when compared to the microfluidic-assisted electrospinning. Regarding PVA fibrous meshes processed by the different techniques (Fig. 5b), the stress-strain curve from the microfluidic-assisted electrospinning has a higher tensile stress than the others. Moreover, the PVA curves are also, generally, characterized by a lower tensile stress as well lower strain when compared to the ones obtained with PCL fibrous meshes. On the other hand, PCL + PVA fibrous meshes processed by microfluidic-assisted electrospinning show a higher tensile stress and lower strain than the ones processed by co-axial electrospinning. Moreover, the stress-strain curves of the PVA leaching fibrous meshes are similar to the original ones for both techniques (Fig. 5c).

The mechanical properties of fibrous meshes made of PCL, PVA or their combination processed by conventional, coaxial or microfluidic-assisted electrospinning are presented in Fig. 6. Results show that the Elastic Modulus of PCL fibrous meshes processed by conventional electrospinning was significantly higher when compared with to the ones processed by coaxial electrospinning ($p < 0.05$). When processed by microfluidic-assisted electrospinning, the PCL fibrous meshes presented an Elastic Modulus comparable to the other processing techniques (conventional and coaxial electrospinning). The Elastic Modulus of PVA fibrous meshes processed by conventional was comparable to the ones
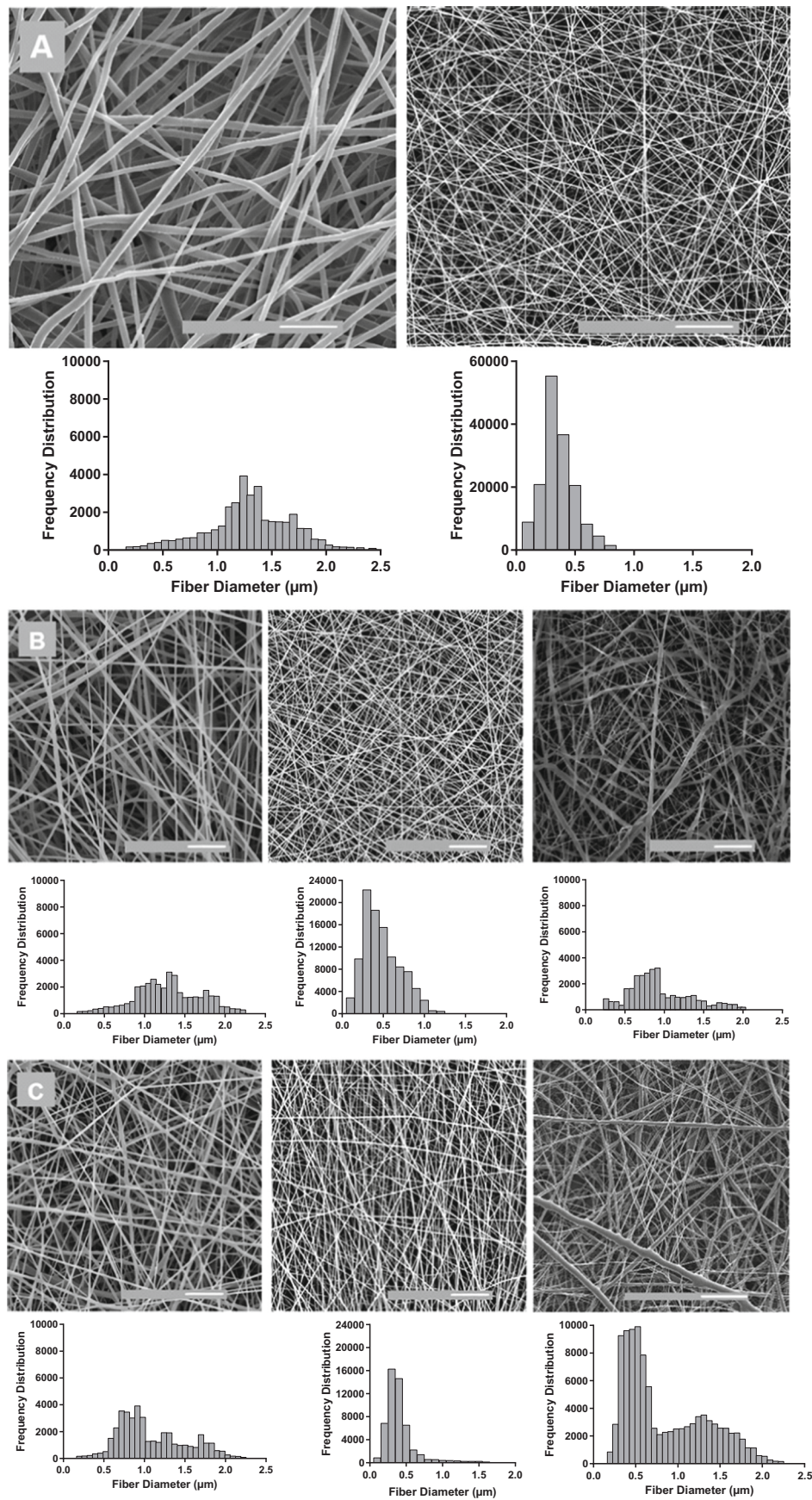
Fig. 3. SEM micrographs (×2000 magnification) and the corresponding fiber diameter histograms of a) conventional electrospinning (experimental control) of PCL and PVA; b) coaxial electrospinning of PCL (shell), PVA (core) and full coaxial electrospinning; and c) microfluidic-assisted electrospinning of PCL, PVA and PCL + PVA. Scale bar: 10 μm.
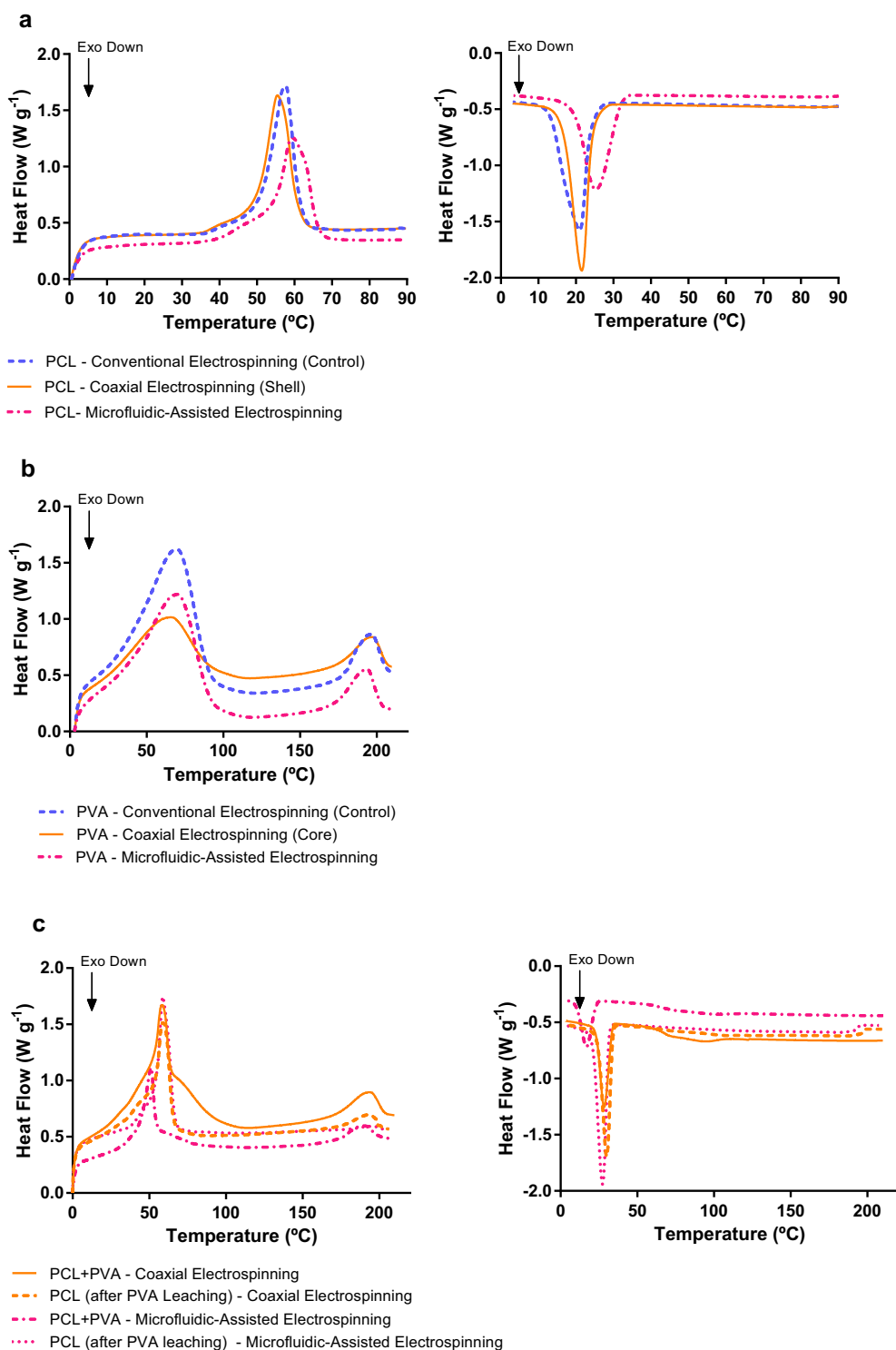
Fig. 4. Representative DSC curves of a) PCL fibrous meshes processed by conventional (control), coaxial (shell), and microfluidic-assisted electrospinning; b) PVA fibrous meshes processed by conventional (control), coaxial (core), and microfluidic-assisted electrospinning, and c) PCL + PVA fibrous meshes processed by coaxial, microfluidic-assisted electrospinning, and after PVA leaching (24 h immersion in water). Images on the left represent the heating cycle and on the right the cooling cycle.

a

- - - PCL - Conventional Electrospinning (Control)
—— PCL - Coaxial Electrospinning (Shell)
-·-· PCL- Microfluidic-Assisted Electrospinning

b

- - - PVA - Conventional Electrospinning (Control)
—— PVA - Coaxial Electrospinning (Core)
-·-· PVA - Microfluidic-Assisted Electrospinning

c

—— PCL+PVA - Coaxial Electrospinning
- - - PCL (after PVA Leaching) - Coaxial Electrospinning
-·-· PCL+PVA - Microfluidic-Assisted Electrospinning
······ PCL (after PVA leaching) - Microfluidic-Assisted Electrospinning

processed by coaxial electrospinning, and by microfluidic-assisted electrospinning. Moreover, the Elastic Modulus of PVA fibrous meshes processed by coaxial electrospinning was significantly higher than the ones made only of PCL ($p < 0.01$), the ones of PCL (shell) and PVA (core) ($p < 0.05$), and after PVA leaching ($p < 0.05$). Between all other coaxial electrospinning conditions, no statistical differences were observed. The Elastic Modulus of PVA fibrous meshes processed by microfluidic-assisted electrospinning was significantly higher than the ones made only of PCL ($p < 0.001$), the PCL + PVA ($p < 0.01$), and after PVA leaching ($p < 0.01$). Lastly, the Elastic Modulus of PCL fibrous meshes

processed by microfluidic-assisted electrospinning was also significantly lower the PCL + PVA ($p < 0.05$), and after PVA leaching ($p < 0.05$). Regarding the fibrous meshes subjected to PVA leaching, the ones processed by coaxial electrospinning had a significant lower Elastic Modulus than the ones processed by microfluidic-assisted electrospinning ($p < 0.05$).

Looking at the maximum stress, the PCL fibrous meshes processed by conventional electrospinning were significantly higher than PCL samples (shell) processed by coaxial electrospinning ($p < 0.05$). When processed by microfluidic-assisted electrospinning, the maximum stress

Table 3

Melting (T_m), and crystallization (T_c) peak temperatures, enthalpy of melting (ΔH_m) and crystallization (ΔH_c), of PCL, PVA, PCL + PVA, and PCL (after PVA leaching) fibrous meshes processed by conventional, coaxial, and microfluidic-assisted electrospinning.

	Solutions	T_m [°C]	ΔH_m [J·g^{-1}]	T_c [°C]	ΔH_c [J·g^{-1}]
Conventional electrospinning	PCL	56.2±1.5	28.9±1.4	20.4±1.0	25.4±1.3
	PVA	194.3±0.4	17.8±3.5	–	–
Coaxial electrospinning	PCL (shell)	55.3±1.5	27.8±0.9	21.5±0.5	26.9±0.8
	PVA (core)	191.1±2.9	13.4±1.5	–	–
	PCL + PVA	58.5±0.3 and 182.4±2.5	30.8±0.7 and 17.2±1.4	27.2±1.0	27.3±0.5
	PCL (after PVA leaching)	58.7±0.8	18.3±1.4	33.8±1.9	15.6±1.3
Microfluidic-assisted electrospinning	PCL	56.9±2.5	17.4±0.4	23.6±0.9	20.3±1.2
	PVA	195.1±1.8	11.0±1.0	–	–
	PCL + PVA	54.7±2.7 and 182.1±3.5	26.8±1.9 and 15.5±3.4	15.9±2.1	24.3±0.2
	PCL (after PVA leaching)	59.3±0.3	14.4±2.0	22.5±1.3	13.4±1.9
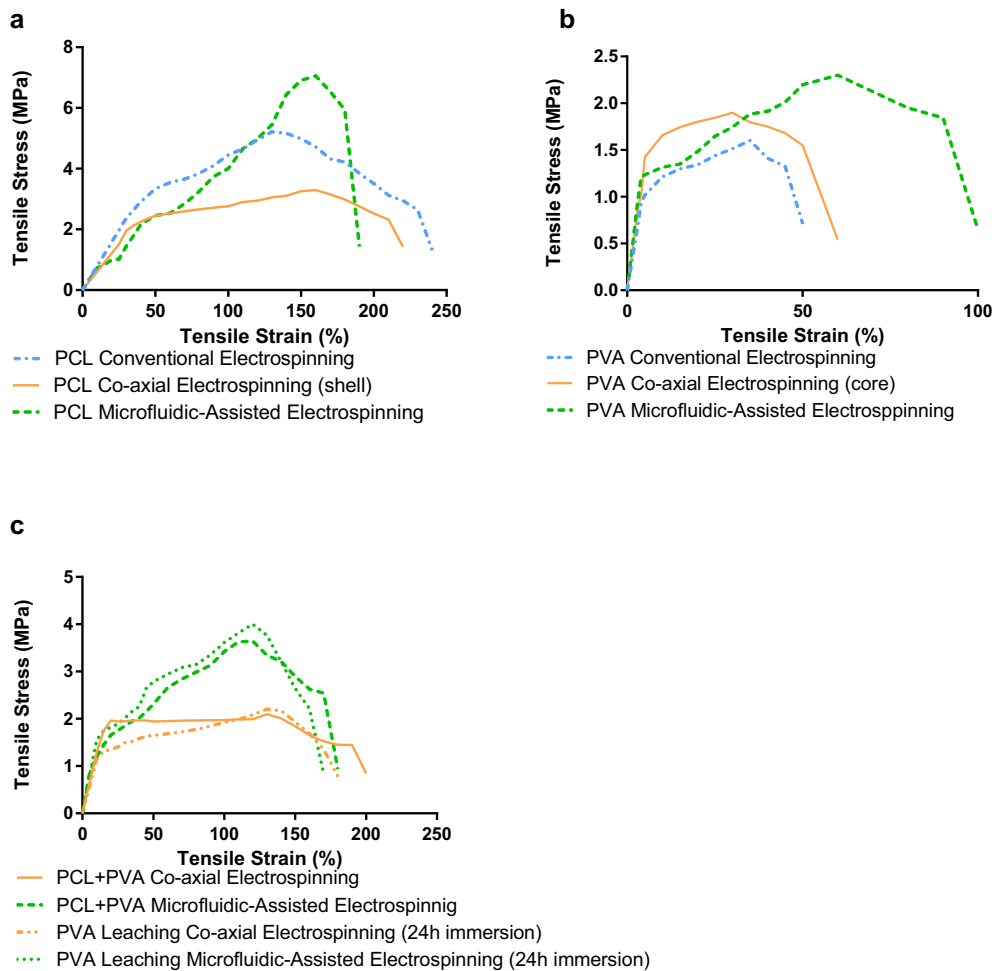
Fig. 5. Representative stress-strain curves of a) PCL fibrous meshes processed by conventional (control), coaxial (shell), and microfluidic-assisted electrospinning; b) PVA fibrous meshes processed by conventional (control), coaxial (core), and microfluidic-assisted electrospinning and c) PCL + PVA fibrous meshes processed by coaxial, microfluidic-assisted electrospinning, and after PVA leaching (24 h immersion in water).

of PCL fibrous meshes significantly increased to 5.89 (5.13–9.60) MPa when compared to coaxial electrospinning ($p < 0.05$). No statistical differences were observed when comparing the maximum stress of PVA samples processed by the different electrospinning techniques. By its side, the maximum stress of PCL + PVA fibrous meshes processed by microfluidic was significantly higher than the ones processed by coaxial electrospinning ($p < 0.05$). The values of the maximum stress for coaxial and microfluidic-assisted electrospun fibrous meshes after PVA leaching did not presented statistical differences. Furthermore, when comparing the values of the maximum stress of the different fibrous meshes processed by coaxial electrospinning, no statistical differences were

observed. A similar observation was found when comparing the different fibrous meshes processed by microfluidic-assisted electrospinning.

When comparing the strain at break, results showed that PCL fibrous meshes processed by microfluidic-assisted electrospinning were significantly lower than the ones processed by conventional electrospinning ($p < 0.001$) and by coaxial electrospinning ($p < 0.05$). Regarding the PVA fibrous meshes, the strain at break of the samples processed by microfluidic-assisted electrospinning were also significantly higher than the ones processed by conventional electrospinning ($p < 0.01$) or coaxial electrospinning ($p < 0.01$). No statistical differences were observed
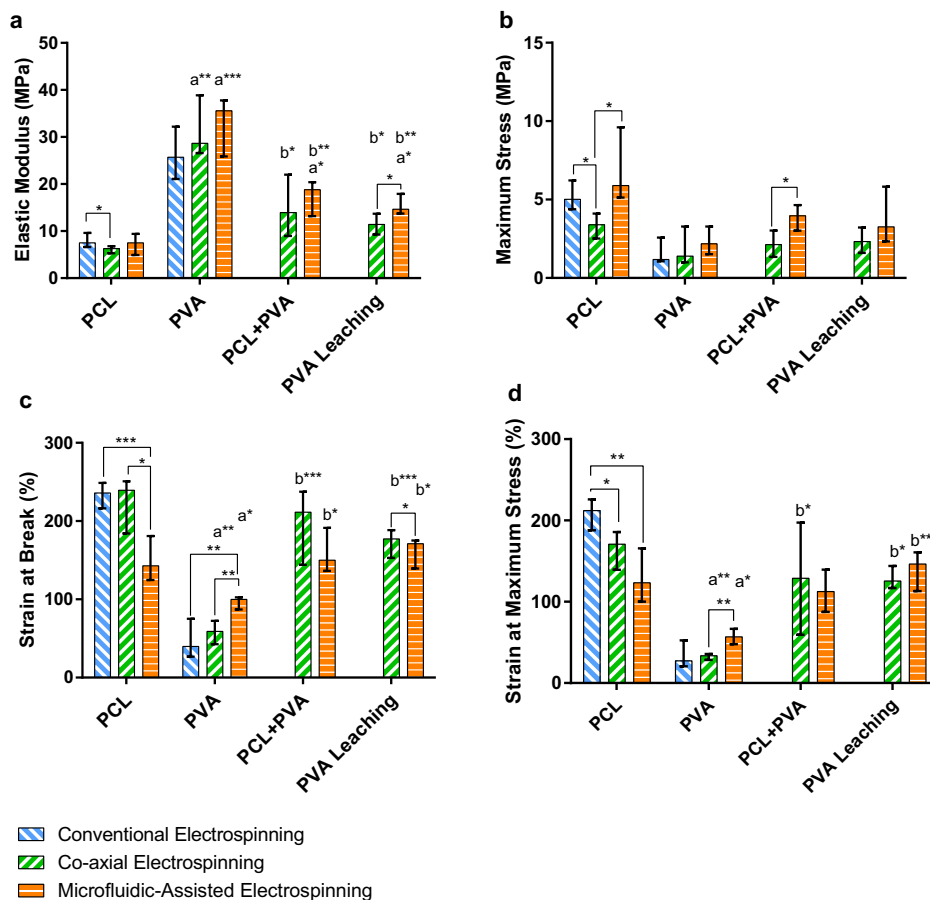
Fig. 6. Uniaxial Tensile Properties of PCL, PVA, PCL + PVA and PVA leaching fibrous meshes processed by conventional, coaxial, or microfluidic-assisted electrospinning: a) Elastic Modulus, b) maximum stress, c) strain at break, and d) strain at maximum stress. Data were analyzed by the Krustal-Wallis test, followed by Dunn's multiple comparison test for comparisons between the same technique using different materials: a denotes significant differences compared to PCL fibrous meshes processed by coaxial or microfluidic-assisted electrospinning, and b denotes significant differences compared to PVA fibrous meshes processed by coaxial or microfluidic-assisted electrospinning. The Mann-Whitney test was also performed for comparisons between the same material using different techniques. Statistical differences: $*p < 0.05$, $**p < 0.01$, $***p < 0.001$, and $****p < 0.0001$. The data is expressed as median $\pm$ interquartile range.

Legend:
- Conventional Electrospinning
- Co-axial Electrospinning
- Microfluidic-Assisted Electrospinning

when comparing the strain at break of PCL + PVA fibrous meshes processed by coaxial or microfluidic-assisted electrospinning. The values of the strain at break after PVA leaching showed that the fibrous meshes processed by coaxial electrospinning were significantly higher than the ones processed by microfluidic-assisted electrospinning ($p < 0.05$). Furthermore, when comparing the strain at break of all fibrous meshes processed by coaxial electrospinning, results showed that PVA fibrous meshes were significantly lower than the PCL fibrous meshes ($p < 0.0001$), the PCL + PVA fibrous meshes ($p < 0.001$) and the PVA leached fibrous meshes ($p < 0.001$). Lastly, the values of the strain at break of all fibrous meshes processed by microfluidic-assisted electrospinning showed that PVA fibrous meshes were significantly lower than the ones made only of PCL ($p < 0.05$), the PCL + PVA ones ($p < 0.05$), and after PVA leaching ($p < 0.05$).

When comparing the strain at maximum stress, results showed that the PCL fibrous meshes processed by conventional electrospinning was significantly higher than the ones processed by coaxial ($p < 0.05$) or by microfluidic-assisted electrospinning ($p < 0.01$). Regarding the PVA fibrous meshes, the strain at maximum stress of the ones processed by microfluidic-assisted electrospinning was significantly higher than the ones processed by coaxial electrospinning ($p < 0.01$). No statistical differences were observed when comparing the strain at maximum stress of PCL + PVA fibrous meshes processed by coaxial or microfluidic-assisted electrospinning, as well as for the fibrous meshes subject to PVA leaching. Furthermore, when comparing the strain at maximum stress of the different fibrous meshes processed by coaxial electrospinning, the PVA samples were significantly lower than the PCL samples ($p < 0.001$), the PCL + PVA samples ($p < 0.05$) and the PVA leached samples ($p < 0.05$). Lastly, the comparison between the different fibrous meshes processed by microfluidic-assisted electrospinning showed strain at break values for PVA samples significantly lower than the ones

made only of PCL ($p < 0.05$), and after PVA leaching ($p < 0.01$).

3.2. Drug release profiles

The percentages of released MTX and anti-TNFα antibody from the different fibrous meshes can be observed in Fig. 7.

According to Fig. 7a, both microfluidic-assisted conditions showed a higher released concentration of MTX, when compared to coaxial electrospinning meshes. In the first 12 h there was a burst release of MTX. Then, it took up to 11 days to release 59.04% and 74.64% of the initial encapsulated MTX for PCL meshes processed by coaxial and microfluidic-assisted electrospinning, respectively. Regarding coaxial and microfluidic-assisted PCL and PVA electrospun meshes, the released MTX reached 79.80% and 88.72% of the initial drug concentration.

According to Fig. 7b, meshes of PCL and PVA processed by microfluidic-assisted electrospinning showed a higher released concentration of anti-TNFα antibody. Through all the experiment, there was a sustained release in all conditions where the drug was encapsulated. The anti-TNFα antibody released from microfluidic-assisted PVA fibrous meshes was 29.32% of the initial concentration. Regarding coaxial and microfluidic-assisted PCL and PVA electrospun meshes, the anti-TNFα antibody released was 30.02% and 33.40% of its initial concentration, respectively.

The remaining conditions (without the presence of pharmaceutical agents) did not showed any signs of release, as expected.

3.3. Biological assays

3.3.1. Cellular performance over the electrospun fibrous meshes

Different biological assays (metabolic activity, proliferation, GAGs synthesis and cell morphology) were conducted to assess the
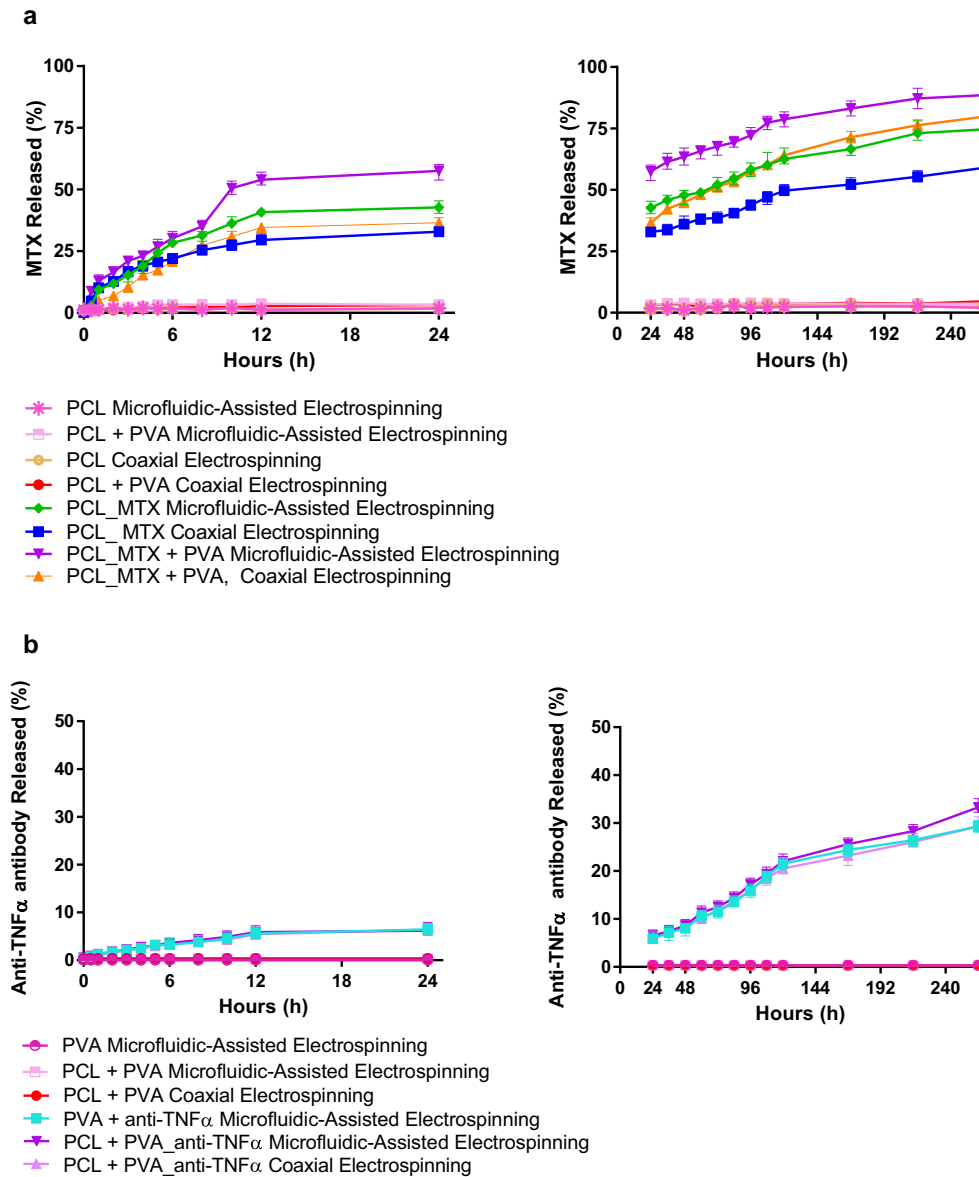
a

- ✳ PCL Microfluidic-Assisted Electrospinning
- ▣ PCL + PVA Microfluidic-Assisted Electrospinning
- ⬡ PCL Coaxial Electrospinning
- ● PCL + PVA Coaxial Electrospinning
- ◆ PCL_MTX Microfluidic-Assisted Electrospinning
- ■ PCL_ MTX Coaxial Electrospinning
- ▼ PCL_MTX + PVA Microfluidic-Assisted Electrospinning
- ▲ PCL_MTX + PVA, Coaxial Electrospinning

b

- ◒ PVA Microfluidic-Assisted Electrospinning
- ▣ PCL + PVA Microfluidic-Assisted Electrospinning
- ● PCL + PVA Coaxial Electrospinning
- ▣ PVA + anti-TNFα Microfluidic-Assisted Electrospinning
- ▼ PCL + PVA_anti-TNFα Microfluidic-Assisted Electrospinning
- ▲ PCL + PVA_anti-TNFα Coaxial Electrospinning

Fig. 7. Quantification of released a) MTX and b) anti-TNFα antibody from the electrospun fibrous meshes.

cytotoxicity of the meshes by culturing them with hACs, since this is the only cell type present in cartilaginous tissues (Fig. 8 and Supplementary Fig. 1).

Experimental results (Fig. 8a) showed that, for the 1st day, PCL + MTX processed by microfluidic-assisted ($p < 0.01$) and coaxial ($p < 0.0001$) electrospinning, and PCL + MTX_PVA + anti-TNFα antibody coaxial electrospun fibrous meshes ($p < 0.01$) displayed a significantly higher cell metabolic activity when compared with all the control conditions without the drugs or with both free drugs. Moreover, fibrous meshes of PCL + MTX_PVA + anti-TNFα antibody processed by microfluidic-assisted electrospinning ($p < 0.001$) and PCL fibrous meshes with free MTX ($p < 0.0001$) also hadsignificantly higher cell metabolic activity than the PCL + PVA fibrous meshes processed by coaxial electrospinning. Lastly, PCL + MTX_PVA + anti-TNFα antibody fibrous meshes processed by microfluidic-assisted electrospinning ($p < 0.05$) presented significantly lower cell metabolic activity than PCL + MTX coaxial meshes. At day 3, control conditions without the drugs and with free drugs displayed a significantly lower cell metabolic activity than PCL + MTX_PVA + anti-TNFα antibody fibrous meshes processed by coaxial electrospinning ($p < 0.001$, $p < 0.01$, $p < 0.0001$, $p < 0.05$,

and $p < 0.001$, respectively). In addition, PCL + MTX fibrous meshes processed by microfluidic-assisted ($p < 0.001$) and coaxial electrospinning ($p < 0.0001$), as well as PCL + MTX_PVA + anti-TNFα antibody fibrous meshes processed by microfluidic-assisted electrospinning ($p < 0.05$), and with free MTX ($p < 0.05$), presented significantly higher cell metabolic activity than PCL + PVA fibrous meshes processed by coaxial electrospinning. Moreover, PCL + MTX fibrous meshes processed by coaxial electrospinning also exhibited significantly higher cell metabolic activity than both free drugs ($p < 0.05$). On the other hand, PCL + MTX_PVA + anti-TNFα antibody fibrous meshes processed by microfluidic-assisted electrospinning showed significantly lower cell metabolic activity than the same ones processed by coaxial electrospinning ($p < 0.05$). Regarding the 7th day of the experiment, results showed a significantly higher cell metabolic activity for PCL + MTX_PVA + anti-TNFα antibody fibrous meshes processed by microfluidic-assisted electrospinning when in comparison with PCL + PVA control meshes processed by microfluidic-assisted and coaxial electrospinning ($p < 0.001$ and $p < 0.0001$, respectively), with PCL + MTX fibrous meshes processed by coaxial electrospinning ($p < 0.05$), and with both control conditions with free MTX ($p < 0.05$) and MTX +

anti-TNFα antibody ($p < 0.0001$). Furthermore, the PCL + PVA fibrous meshes processed by coaxial electrospinning presented significantly lower cell metabolic activity than PCL control fibrous meshes ($p < 0.01$) and PCL + MTX processed by the microfluidic-assisted electrospinning ($p < 0.001$), and PCL + MTX_PVA + anti-TNFα antibody coaxial fibrous meshes ($p < 0.0001$). Lastly, PCL ($p < 0.01$)and PCL + MTX ($p < 0.001$) fibrous meshes processed by microfluidic-assisted electrospinning, and PCL + MTX_PVA + anti-TNFα antibody fibrous meshes processed with coaxial electrospinning ($p < 0.0001$) also displayed significantly higher cell metabolic activity than control conditions with both free drugs. The analysis of the hACs by fluorescence microscopy revealed the typical spherical morphology when cultured over the different electrospun fibrous meshes (Supplementary Fig. 1).

Concerning the quantification of synthesized GAGs (Fig. 8b), on the 1ˢᵗ day of the experiment several statistical differences were observed. The fibrous meshes of PCL + MTX_PVA + anti-TNFα antibody processed by microfluidic-assisted electrospinning displayed a significantly higher GAG concentration, when compared to the three control conditions without drugs ($p < 0.0001$, $p < 0.0001$, and $p < 0.01$), to the PCL + MTX_PVA + anti-TNFα antibody fibrous meshes processed by coaxial electrospinning ($p < 0.05$), and to the two control conditions with free pharmaceutical agents ($p < 0.001$ and $p < 0.0001$). PCL + MTX meshes processed by microfluidic-assisted electrospinning showed a significative increase in the GAGs concentration when compared to the PCL and PCL + PVA control conditions processed by microfluidic-assisted electrospinning ($p < 0.001$, $p < 0.0001$), and to the control conditions with free drugs ($p < 0.01$ and $p < 0.0001$). In addition, PCL + MTX coaxial fibrous meshes also showed significantly higher GAG concentration in comparison to PCL + free MTX_PVA + free anti-TNFα antibody ($p < 0.05$). At day 3, fibrous meshes of PCL + MTX_PVA + anti-TNFα

antibody processed by microfluidic-assisted electrospinning demonstrated a significative increase in GAG concentration, when compared to the three control conditions without drugs ($p < 0.0001$, $p < 0.001$, and $p < 0.01$), PCL + MTX meshes processed by coaxial electrospinning ($p < 0.01$), and the two control conditions with free drugs ($p < 0.001$ and $p < 0.0001$). PCL + MTX microfluidic fibrous had significantly higher concentration of GAGs in comparison to PCL and PCL + PVA control conditions processed by microfluidic-assisted electrospinning ($p < 0.001$, $p < 0.05$), and with PCL + free MTX_PVA + free anti-TNFα antibody ($p < 0.0001$). Moreover, PCL with free MTX fibrous also showed significantly higher GAG concentration in comparison to PCL + free MTX_ PVA + free anti-TNFα antibody ($p < 0.01$). At the 7ᵗʰ day of the assay, fibrous meshes of PCL + MTX_PVA + anti-TNFα antibody processed by microfluidic-assisted electrospinning demonstrated a significative increase in GAG concentration, when compared to the three control conditions without drugs ($p < 0.0001$, $p < 0.0001$, and $p < 0.05$), the PCL + MTX meshes processed by coaxial electrospinning ($p < 0.05$), and the two control conditions with free drugs ($p < 0.001$ and $p < 0.0001$). PCL meshes processed by microfluidic-assisted electrospinning displayed significantly lower GAG concentration in comparison to PCL + MTX processed by microfluidic-assisted electrospinning ($p < 0.05$), and with PCL with free MTX fibrous meshes ($p < 0.05$). Lastly, PCL + free MTX_PVA + free anti-TNFα meshes also had a significative decrease in GAGs concentration when compared to the PCL + MTX fibrous mesh processed by microfluidic ($p < 0.001$) and coaxial electrospinning ($p < 0.01$), and with free MTX ($p < 0.001$).

Regarding dsDNA quantification results (Fig. 8c), no statistical differences were found between the three control conditions without drugs throughout the experiment. At the 1ˢᵗ day, there was a significant increase in cell proliferation when comparing PCL + MTX_PVA + anti-
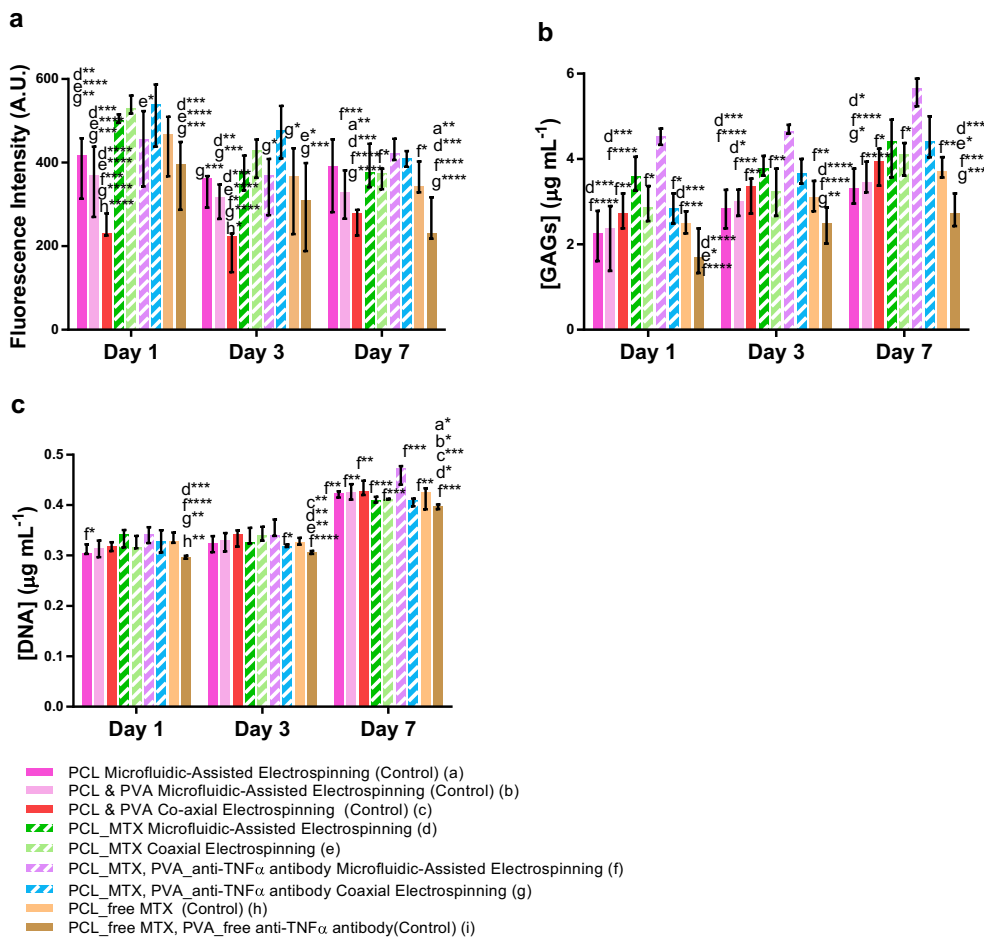
Fig. 8. Biological assays conducted on the fibrous meshes seeded with hACs. a) Cell metabolic activity by Alamar blue; b) GAG quantification; and c) cell proliferation dsDNA quantification. Data were analyzed by the Krustal-Wallis test, followed by Dunn's multiple comparison test for: *a* denotes significant differences compared to PCL microfluidic fibrous meshes, *b* denotes significant differences compared to PCL + PVA meshes created with microfluidic-assisted electrospinning, *c* denotes significant differences compared to PCL + PVA processed by coaxial electrospinning, *d* denotes significant differences compared to PCL fibrous meshes processed microfluidic-assisted electrospinning with encapsulated MTX, *e* denotes significant differences compared to PCL fibrous meshes processed by coaxial electrospinning with encapsulated MTX, *f* denotes significant differences compared to PCL and PVA fibrous meshes processed by microfluidic-assisted electrospinning with encapsulated MTX and anti-TNF-α antibody, *g* denotes significant differences compared to PCL and PVA fibrous meshes processed by coaxial electrospinning with encapsulated MTX and anti-TNFα antibody, and *h* denotes significant differences compared to PCL with free MTX. Statistical differences: *$p < 0.05$, **$p < 0.01$, ***$p < 0.001$, and ****$p < 0.0001$. The data is expressed as median ± interquartile range.

Legend:
- PCL Microfluidic-Assisted Electrospinning (Control) (a)
- PCL & PVA Microfluidic-Assisted Electrospinning (Control) (b)
- PCL & PVA Co-axial Electrospinning (Control) (c)
- PCL_MTX Microfluidic-Assisted Electrospinning (d)
- PCL_MTX Coaxial Electrospinning (e)
- PCL_MTX, PVA_anti-TNFα antibody Microfluidic-Assisted Electrospinning (f)
- PCL_MTX, PVA_anti-TNFα antibody Coaxial Electrospinning (g)
- PCL_free MTX (Control) (h)
- PCL_free MTX, PVA_free anti-TNFα antibody(Control) (i)

ARTICLE IN PRESS

F. Vasconcelos et al.   Materials Science & Engineering C xxx (xxxx) xxx

TNFα antibody fibrous meshes with PCL fibrous meshes both processed by microfluidic-assisted electrospinning ($p < 0.05$), and with the free drugs conditions ($p < 0.0001$). In addition, both free drugs also presented significantly lower DNA concentrations than the PCL + MTX fibrous meshes processed by microfluidic-assisted electrospinning ($p < 0.001$), the PCL + MTX_PVA + anti-TNFα antibody fibrous meshes processed by coaxial electrospinning ($p < 0.01$), and with free MTX ($p < 0.01$). At the 3$^{\text{rd}}$ day, there was a significant increase in cell proliferation when comparing PCL + MTX_PVA + anti-TNFα antibody fibrous meshes processed by microfluidic-assisted electrospinning with PCL + MTX_PVA + anti-TNFα antibody processed coaxial electrospinning ($p < 0.05$) and PCL + PVA with free drugs meshes ($p < 0.0001$). Furthermore, PCL + PVA with free pharmaceutical agents also presented significantly lower cell proliferation than the PCL + PVA fibrous meshes processed by coaxial ($p < 0.01$), and the PCL + MTX fibrous meshes processed by microfluidic ($p < 0.01$) and coaxial electrospinning ($p < 0.01$). On the last day of the experiment, PCL + MTX_PVA + anti-TNFα antibody processed by microfluidic-assisted electrospinning displayed a DNA concentration significantly higher than all the other conditions: the three controls without pharmaceutical agents ($p < 0.01$), PCL + MTX fibrous meshes processed by microfluidic and coaxial electrospinning ($p < 0.001$), PCL + MTX_PVA + anti-TNFα antibody processed by coaxial electrospinning ($p < 0.001$), and control conditions with free drugs ($p < 0.01$ and $p < 0.001$). Lastly, PCL + PVA with free pharmaceutical agents also presented significantly lower cell proliferation than the PCL ($p < 0.05$) and the PCL + PVA ($p < 0.05$) fibrous meshes processed by microfluidic-assisted electrospinning, the PCL + PVA fibrous meshes processed by coaxial electrospinning ($p < 0.001$), and the PCL + MTX fibrous meshes processed by microfluidic-assisted electrospinning ($p < 0.05$).

The metabolic activity and proliferation of THP-1 cells was also assessed (Fig. 9).

Regarding the cell metabolic activity (Fig. 9a) there was a significant increase on day 1, when comparing PCL + MTX, and PCL + MTX_PVA + anti-TNFα antibody fibrous meshes processed by microfluidic-assisted electrospinning with PCL + MTX ($p < 0.01$ and $p < 0.001$) and PCL + MTX_PVA + anti-TNFα antibody ($p < 0.01$ and $p < 0.0001$) coaxial fibrous meshes, and with the controls with free drugs ($p < 0.01$ and $p < $

0.0001). Cell metabolic activity of the control condition with both free drugs was also significantly lower than the one obtained for all the control conditions without pharmaceutical agents ($p < 0.0001$), as well for the THP-1 conditioned medium ($p < 0.001$). At the 3$^{\text{rd}}$ day, there was a significative decrease in THP-1 metabolic activity when comparing the controls with the free drugs (p < 0.01, p < 0.0001, p < 0.01, and p < 0.0001). The free drugs also presented a significative decrease in comparison to the PCL + MTX, and the PCL + MTX_PVA + anti-TNFα antibody fibrous meshes processed by microfluidic and coaxial electrospinning, as well with the THP-1 conditioned medium. In addition, THP-1 conditioned medium ($p < 0.05$) and the PCL + MTX_PVA + anti-TNFα antibody fibrous meshes ($p < 0.01$) processed by microfluidic-assisted electrospinning displayed a significative higher cell metabolic activity than PCL + MTX fibrous meshes processed by coaxial electrospinning. At day 7, results displayed a significative increase in cell metabolic activity when comparing PCL + MTX_PVA + anti-TNFα antibody fibrous meshes processed by microfluidic-assisted electrospinning, with THP-1 conditioned medium, PCL + PVA ($p < 0.01$ and $p < 0.01$) and PCL + MTX ($p < 0.01$ and $p < 0.01$) processed by coaxial electrospinning, as well with controls with free drugs (MTX, $p < 0.0001$; MTX_anti-TNFα antibody, $p < 0.0001$). Furthermore, cell metabolic activity was significantly higher on the PCL + MTX_PVA + anti-TNFα antibody fibrous meshes processed by coaxial electrospinning, than the free MTX ($p < 0.05$). Lastly, THP-1 metabolic activity was significatively lower when comparing the meshes with both free drugs ($p < 0.05$, $p < 0.05$, and $p < 0.001$) with PCL and PCL + MTX microfluidic fibrous meshes, and PCL + MTX_PVA + anti-TNFα antibody fibrous meshes processed by coaxial electrospinning.

Concerning dsDNA quantification results (Fig. 9b), no statistical differences were found between the three control conditions without drugs throughout the experiment. At the 1$^{\text{st}}$ day, there was a significant increase in cell proliferation when comparing PCL ($p < 0.05$ and $p < 0.01$), PCL + MTX – ($p < 0.01$ and $p < 0.001$) and PCL + MTX_PVA + anti-TNFα antibody ($p < 0.0001$ and $p < 0.0001$) fibrous meshes processed by microfluid electrospinning with PCL + MTX_PVA + anti-TNFα antibody fibrous meshes processed by coaxial electrospinning ($p < 0.05$ and $p < 0.01$). The THP-1 conditioned medium ($p < 0.0001$ and $p < 0.0001$) induced a significantly higher proliferation than the PCL + MTX
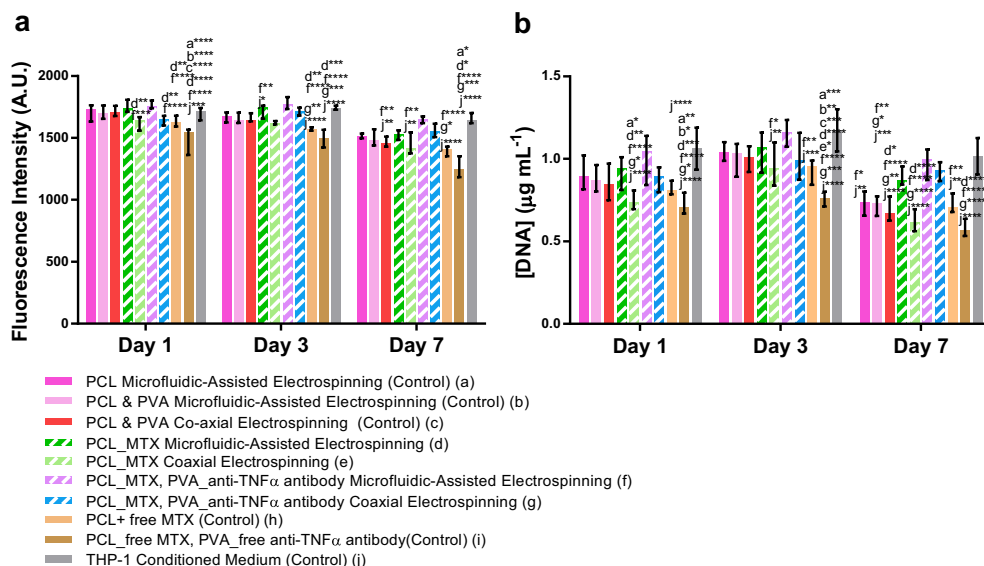
Fig. 9. Biological assays conducted on the fibrous meshes seeded with THP-1. a) Cell metabolic activity determined by Alamar blue assay and b) cell proliferation determined by dsDNA quantification. Data were analyzed by the Krustal-Wallis test, followed by Dunn's multiple comparison test for: *a* denotes significant differences compared to PCL meshes produced by microfluidic-assisted electrospinning, *b* denotes significant differences compared to PCL + PVA fibrous meshes processed by microfluidic-assisted electrospinning, *c* denotes significant differences compared to PCL + PVA meshes created with coaxial electrospinning, *d* denotes significant differences compared to PCL fibrous meshes processed with microfluidic-assisted electrospinning with encapsulated MTX, *e* denotes significant differences compared to PCL fibrous meshes processed by coaxial electrospinning with encapsulated MTX, *f* denotes significant differences compared to PCL and PVA fibrous meshes processed by microfluidic-assisted electrospinning with encapsulated MTX and anti-TNF-α antibody, *g* denotes significant differences compared

Legend:
- PCL Microfluidic-Assisted Electrospinning (Control) (a)
- PCL & PVA Microfluidic-Assisted Electrospinning (Control) (b)
- PCL & PVA Co-axial Electrospinning (Control) (c)
- PCL_MTX Microfluidic-Assisted Electrospinning (d)
- PCL_MTX Coaxial Electrospinning (e)
- PCL_MTX, PVA_anti-TNFα antibody Microfluidic-Assisted Electrospinning (f)
- PCL_MTX, PVA_anti-TNFα antibody Coaxial Electrospinning (g)
- PCL+ free MTX (Control) (h)
- PCL_free MTX, PVA_free anti-TNFα antibody(Control) (i)
- THP-1 Conditioned Medium (Control) (j)

to PCL and PVA fibrous meshes processed by coaxial electrospinning with encapsulated MTX and anti-TNF-α antibody, and *j* denotes significant differences between THP-1 conditioned medium. Statistical differences: *$p < 0.05$, **$p < 0.01$, ***$p < 0.001$, and ****$p < 0.0001$. The data is expressed as median $\pm$ interquartile range.

fibrous meshes processed by coaxial electrospinning and with both free drugs. In the last-mentioned condition, the DNA concentration was also significative lower than PCL + PVA control meshes processed by microfluidic-assisted electrospinning ($p < 0.05$). In addition, THP-1 conditioned medium displayed significative higher mitogenic activity than free MTX ($p < 0.0001$). Cell proliferation at day 3 displayed a significant increase when comparing PCL + MTX_PVA + anti-TNFα antibody fibrous meshes processed by microfluidic-assisted electrospinning ($p < 0.05$, $p < 0.01$ and $p < 0.0001$), and THP-1 conditioned medium ($p < 0.05$, $p < 0.001$, and $p < 0.0001$) with PCL + MTX fibrous meshes processed by coaxial electrospinning and with free drugs. Furthermore, the DNA concentrations in the control free drugs were significantly lower than the ones obtained for PCL ($p < 0.001$), PCL + PVA ($p < 0.01$), and PCL + MTX ($p < 0.0001$) fibrous meshes processed by microfluidic-assisted electrospinning, and PCL + PVA ($p < 0.001$), PCL + MTX ($p < 0.05$), and PCL + MTX_PVA + anti-TNFα antibody – ($p < 0.001$) fibrous meshes processed by coaxial electrospinning. On the last day of the experiment, cell proliferation was significantly higher for PCL + MTX_PVA + anti-TNFα antibody fibrous meshes processed by microfluidic-assisted electrospinning ($p < 0.05$, $p < 0.01$, $p < 0.0001$, $p < 0.0001$, $p < 0.01$, $p < 0.0001$) and THP-1 conditioned medium ($p < 0.01$, $p < 0.001$, $p < 0.0001$, $p < 0.0001$, $p < 0.01$, $p < 0.0001$), when compared to the three controls without drugs, PCL + MTX fibrous meshes processed by coaxial electrospinning, and both controls with free drugs. In addition, PCL + MTX_PVA + anti-TNFα antibody coaxial fibrous meshes ($p < 0.05$, $p < 0.01$, $p < 0.0001$, and $p < 0.0001$) also had a significant increase in their mitogenic activity when compared to the PCL + PVA control conditions, PCL + MTX coaxial meshes, and PCL + free MTX_PVA + free anti-TNFα antibody meshes. Lastly, PCL + MTX fibrous meshes processed by microfluidic-assisted electrospinning presented significatively higher cell proliferation in comparison to PCL + PVA ($p < 0.05$), PCL + MTX ($p < 0.0001$), coaxial meshes, and the control condition with both free drugs ($p < 0.0001$).

3.3.2. Bioactivity of released drugs over TNFα and IL-6

The concentrations of IL-6 and TNFα presented in the conditioned medium of THP-1 cells, upon exposure to the different fibrous meshes, is represented on Fig. 10.

Looking at the IL-6 concentrations (Fig. 10a), there was a significant decrease for all the fibrous meshes encapsulating drugs and all the experiment time points: PCL + MTX ($p < 0.01$) and PCL + MTX_PVA +

anti-TNFα antibody ($p < 0.0001$) processed by microfluidic -assisted electrospinning; and PCL + MTX ($p < 0.01$, $p < 0.05$) and PCL + MTX_PVA + anti-TNFα ($p < 0.05$, $p < 0.001$, and $p < 0.01$) processed by coaxial electrospinning, in comparison to the THP-1 conditioned medium. At day 1, a significant higher reduction of IL-6 concentrations was also noticed in fibrous meshes of PCL + MTX_PVA + anti-TNFα antibody processed by microfluidic-assisted electrospinning, when compared to the control conditions of PCL + PVA fibrous meshes processed by microfluidic ($p < 0.05$) and coaxial ($p < 0.01$) electrospinning. Regarding the day 3, a significant decrease of the IL-6 concentration was also observed between the PCL + MTX_PVA + anti-TNFα antibody processed by microfluidic-assisted electrospinning and the control conditions of PCL microfluidic ($p < 0.05$) and PCL + PVA coaxial electrospinning ($p < 0.01$). Another significant reduction ($p < 0.01$) of IL-6 concentration was also found between the PCL + MTX_PVA + anti-TNFα antibody condition and the PCL + PVA condition, both processed by coaxial electrospinning. In the last day of the experiment, significantly lower values of IL-6 concentration were observed when comparing fibrous meshes of PCL + MTX_PVA + anti-TNFα antibody processed by microfluidic-assisted electrospinning with the control conditions of coaxial fibers without any drugs ($p < 0.001$), as well with free MTX ($p < 0.01$). This significant decrease was also noticed between the PCL + MTX fibrous meshes processed by microfluidic-assisted electrospinning and the control condition PCL + PVA processed by co-axial electrospinning ($p < 0.05$). The concentration of TNFα (Fig. 10b) in the presence of PCL + MTX ($p < 0.05$), and PCL + MTX_PVA + anti-TNFα antibody ($p < 0.01$) fibrous meshes processed by microfluidic-assisted electrospinning decreased significantly throughout the experiment, in comparison to the THP-1 conditioned medium. A significant decrease of TNFα concentration was also observed, at days 3 and 7, for the PCL + MTX fibrous meshes processed by coaxial electrospinning ($p < 0.01$ and $p < 0.001$), respectively, and at day 7 for PCL + MTX_PVA + anti-TNFα antibody coaxial fibrous meshes ($p < 0.01$), in comparison with the THP-1 conditioned medium. In addition, TNFα concentration was also significantly lower when comparing the PCL + MTX coaxial fibrous meshes with free drugs ($p < 0.05$), at the 7th day of the experiment. It is also important to notice that, in both assays, no statistical differences were found between all the control conditions along the time.
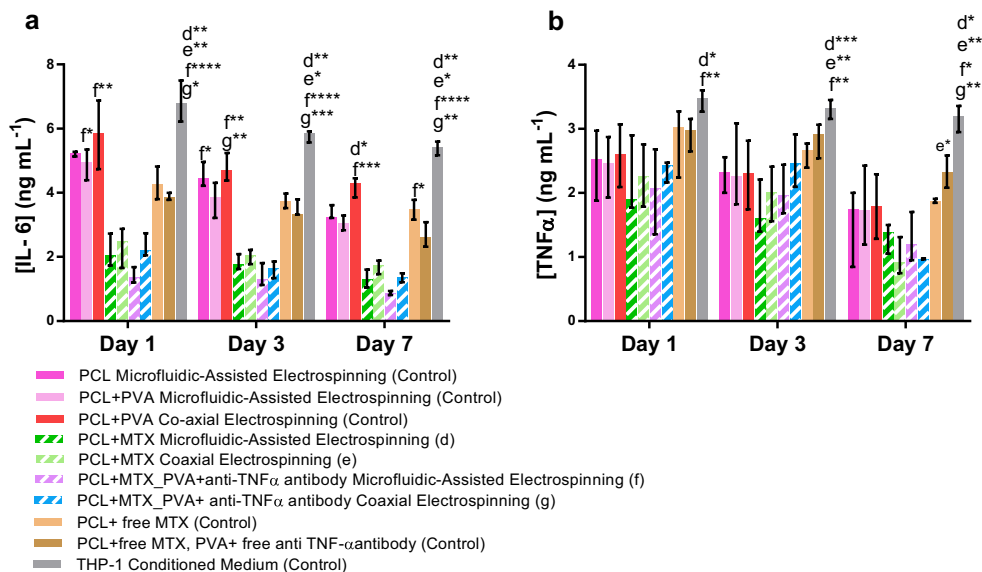
Fig. 10. Concentration of a) IL-6 and b) TNF-α in the conditioned medium of THP-1 cells, cultured in the presence of the different fibrous meshes during 7 days. Data were analyzed by the Krustal-Wallis test, followed by Dunn's multiple comparison test for: d denotes significant differences compared to PCL fibrous meshes processed with microfluidic-assisted electrospinning with encapsulated MTX, e denotes significant differences compared to PCL fibrous meshes processed by coaxial electrospinning with encapsulated MTX, f denotes significant differences compared to PCL and PVA fibrous meshes processed by microfluidic-assisted electrospinning with encapsulated MTX and anti- TNF-α antibody, and g denotes significant differences compared to PCL and PVA fibrous meshes processed by coaxial electrospinning with encapsulated MTX and anti- TNF-α antibody. Statistical differences: *$p < 0.05$, **$p < 0.01$, ***$p < 0.001$, and ****$p < 0.0001$. The data is expressed as median ± interquartile range.

Legend:
- PCL Microfluidic-Assisted Electrospinning (Control)
- PCL+PVA Microfluidic-Assisted Electrospinning (Control)
- PCL+PVA Co-axial Electrospinning (Control)
- PCL+MTX Microfluidic-Assisted Electrospinning (d)
- PCL+MTX Coaxial Electrospinning (e)
- PCL+MTX_PVA+anti-TNFα antibody Microfluidic-Assisted Electrospinning (f)
- PCL+MTX_PVA+ anti-TNFα antibody Coaxial Electrospinning (g)
- PCL+ free MTX (Control)
- PCL+free MTX, PVA+ free anti TNF-αantibody (Control)
- THP-1 Conditioned Medium (Control)

4. Discussion

Inflammatory arthritic diseases are responsible for joint weakness and pain which lead to progressive musculoskeletal disability and serious mobility limitations [1,30]. There is no cure to these diseases and the available treatment strategies aim to achieve a low disease activity state or possible clinical remission through treatment adjustments. Nowadays pharmacological therapies using DMARDs [4,31], specially MTX, are used as gold-standard treatments since they can target inflammation and hinder cartilage degeneration [5]. This drug can be also used in combination with biological DMARDs such as tumor necrosis factor (TNF) inhibitors [1,32,33], aiming to optimize the therapeutics efficacy over non-target tissues. Despite the advances, a systemic drug administration of DMARDs is associated with severe side effects such as nausea, skin reactions, liver (end-stage liver disease), lung (sores) or gastrointestinal tract (diarrhea, infectious disease of the mouth or ulcerative stomatitis) problems [34]. Aiming to circumvent such drawbacks, herein are proposed local controlled dual drug release systems encapsulating MTX and anti-TNFα antibody, which were processed by coaxial and microfluidic-assisted electrospinning. The latest, is a novel technique that allows a continuous exchange of two working fluids, instead of presenting a core-shell structure, as the previous drug release method – coaxial electrospinning.

Prior to drug release and *in vitro* testing, characterization of conventional, coaxial and microfluidic-assisted electrospun fibrous meshes was performed in order to confirm the presence and influence of each polymer used. Concerning the morphology, electrospun fibers had a random orientation and do not had visible defects, as confirmed by SEM micrographs. Furthermore, the PCL fibers were thicker than the PVA ones, since PCL fibers' diameter were mostly between 1 and 1.5 μm, whereas the diameter of PVA fibers were, in their majority, lower than 0.5 μm. Moreover, the fibrous meshes made of both polymers and processed by microfluidic-assisted electrospinning had two distinct populations of fibers' diameter. Fluorescence microscopy images of coaxial fibrous meshes confirmed the presence of an external shell made of PCL and a smaller inner core made of PVA, fitting perfectly one inside the other. The fibrous structure processed by microfluidic-assisted electrospinning with both polymers was confirmed by the presence of both green and red fluorescent dyes easily distinguishable from each other.

DSC results corroborate these fluorescence microscopy observations, since the peaks displayed on the curves and the corresponding values (i.e. melting and crystallization temperatures) are in agreement with the ones described in the literature [35–37]. It is also important to notice that the type of electrospinning technique affected the thermal properties of the fibrous meshes. The enthalpy of the event is determined by the integration of the area under the DSC curve peak. PCL fibrous meshes processed by microfluidic-assisted electrospinning had a small peak area than the ones processed by conventional or coaxial electrospinning, despite the similar values of melting and crystallization temperatures. We assume that the first peaks of Fig. 3b are due to the evaporation of water that masks the glass transition of the PVA that, according to the literature, for PVA (87–89% hydrolyzed) is approximately 60 °C [37]. In addition, the enthalpy of these peaks is very large if compared to the enthalpy of the melting, meaning that it is associated with a phenomenon having a large specific enthalpy, as for the water is. Furthermore, PVA fibrous meshes had a small peak area for microfluidic-assisted electrospinning regarding their melting phase. These small peak areas were also corresponding to smaller enthalpy of melting values. When comparing the DSC from microfluidic and coaxial electrospinning, it can be observed that the curve of coaxial electrospinning has large peak area than the ones of microfluidic-assisted electrospinning, resulting in higher values of melting and crystallization enthalpies. Moreover, after the immersion of coaxial and microfluidic-assisted electrospinning fibrous meshes in water, the melting and crystallization tempeartures were similar, although a little smaller for microfluidic, respectively. No corresponding peak to water content was observed in the DSC curves,

which confirm the leaching of PVA, since the obtained curves and temperature values correspond to the ones of PCL [35].

The uniaxial tensile properties of PCL or PVA fibrous meshes were found to be significantly different for each electrospinning processing technique. The PCL fibers presented the lower Elastic Modulus between all tested conditions, although the other mechanical properties (i.e. maximum stress, strain at break and at maximum stress) were the highest, as reported by others [38,39]. Regarding the mechanical properties of fibrous meshes processed by coaxial or microfluidic-assisted electrospinning, it was observed a trend to behave similarly to conventional PCL fibrous meshes. In addition, those fibrous meshes do not have significant differences between each other, apart from the maximum stress, that is significantly higher when processed by microfluidic-assisted electrospinning. Upon PVA leaching, the fibrous meshes have similar properties to the ones processed with both polymers. This means that, although one of the polymers was leached out, the fibrous meshes are still able to maintain their integrity, without losing their mechanical properties. When comparing the Elastic Modulus of the processed fibrous meshes with the Elastic Modulus of human tissues, it was found to be within the range of values found for cartilage tissues (5–15 MPa) [40,41], especially the PCL and PCL + PVA fibrous meshes (between 5.3 and 20.4 MPa).

After characterizing the different fibrous meshes processed by coaxial and microfluidic-assisted electrospinning, MTX and anti-TNFα antibody were encapsulated at concentrations within the range clinically approved for the treatment of inflammatory arthritic diseases. MTX has proved to be a strong inhibitor of inflammation, inducing a reduction on the production of several cytokines (such as TNFα and IL-6), as well as modulating T cell activation [42,43]. Moreover, the combination of MTX with biological DMARDs, in this case anti-TNFα antibody, has also been established as an efficient biopharmaceutical strategy for the treatment of these diseases, since the antibody is capable of blocking TNF signaling or block the interaction of TNF with their respective receptors [44], having a synergistic therapeutic effect. Release studies demonstrated that both microfluidic conditions allowed a higher released concentration of MTX, when compared to the co-axial electrospinning. The release of higher concentrations of MTX on microfluidic conditions can be explained by the fact that these fibrous meshes are made of solid fibers, instead of hollow fibers as the ones obtained by coaxial electrospinning. In fact, microfluidic fibrous meshes of PCL and PCL + PVA also demonstrated to have a lower diameter than the ones processed by coaxial, which comprise a higher the surface area to volume ratio [45]. This emphasizes why microfluidic-assisted electrospinning fibrous meshes with encapsulated MTX have a higher drug release than the coaxial ones [46]. Regarding the anti-TNFα antibody, it was observed a sustained and linear release into both coaxial (core) and microfluidic-assisted electrospinning fibrous meshes. Although the microfluidic systems showed a higher concentration, the antibody release seems to be retained along time, since its diffusivity is restricted due to the high molecular weight, as previously reported for other proteins [19,46,47]. In addition, upon PVA dissolution, there is the formation of a hydrated gel-like structure around or inside the PCL fibers, which also contributes to the obstruction in the diffusion of encapsulated drugs, restricting their complete release [48]. In addition, the proposed system also demonstrated the possibility to encapsulate and deliver drugs with different solubility behavior. In particular, a drug soluble in organic solvents with the PCL fiber and a water-soluble drug with the PVA fiber.

After the successful encapsulation of both drugs into microfluidic and coaxial electrospun fibrous meshes, their cytotoxicity and efficacy was tested with hACs and THP-1 cells, respectively. The cytotoxicity results showed that, in general, the fibrous meshes with the encapsulated drugs have significantly higher hACs metabolic activity, when compared with the controls without any pharmaceutical agent or even free drugs. Regarding cell morphology, seeded cells display their normal round shape when cultured over the different fibrous meshes. Moreover,

the PCL + MTX_PVA + anti-TNFα antibody fibrous meshes processed by microfluidic-assisted electrospinning displayed significantly higher GAG synthesis and hACs proliferation than all the control conditions, namely the condition with both free drugs. This demonstrates that the proposed system is not cytotoxic to chondrocytic cells and does not compromise their normal activity. Most likely, the encapsulated drugs have less side effects than when administered freely. Therefore, the proposed controlled dual drug release system represents a safer therapeutic strategy for the treatment of inflammatory arthritic diseases.

THP-1 cells were also used as an *in vitro* model of human monocytes and macrophages capable of simulating an inflammatory environment, especially after their stimulation with inflammatory activators [49]. Accordingly, the produced fibrous meshes were tested in the presence of THP-1 cells stimulated with LPS. The efficacy of the proposed controlled dual drug release system was demonstrated by the significant decrease in the concentration levels of the pro-inflammatory cytokines TNF and IL-6 in the conditions where MTX or MTX and anti-TNFα antibody were encapsulated. A more accentuated decrease in both cytokines' concentrations is observed in the fibrous meshes with both pharmaceutical agents processed by microfluidic-assisted electrospinning.

Altogether, these scientific evidences support the aim of developing a local controlled dual drug release system which may help to solve some of the major shortcomings of systemic administration. Particularly, fibrous meshes processed by microfluidic-assisted electrospinning have reduced drugs' side effects and maintain their therapeutic concentrations over a longer time [50]. The fibrous meshes with the encapsulated drugs can be implanted in the body through a minimally invasive surgical joint procedure called arthroscopy. In addition, the implantation of the fibrous meshes will be fundamental to decrease the inflammation, due to the release of the pharmaceutical agents that will remain in site aiming to support, and, ultimately, promote cartilage regeneration.

5. Conclusion

A controlled dual drug release system was herein developed by encapsulating MTX and anti-TNFα antibody into fibrous meshes processed by a novel technique called microfluidic-assisted electrospinning. Although the fibrous meshes processed by microfluidic and coaxial electrospinning had distinct morphological characteristics, their uniaxial tensile properties are similar to each other. Indeed, their Elastic Modulus is within the range of human articular cartilage. Accordingly, hACs were seeded on electrospun fibrous meshes and no cytotoxic effect was observed. Interestingly, they were able to induce a higher GAGs synthesis.

Although drug release studies show that MTX and, in particular, anti-TNFα antibody are not fully released, their efficacy is confirmed by a significant reduction of TNFα and IL-6 concentrations in conditioned medium of stimulated THP-1 cells. Particularly, more accentuated decreases are shown in the meshes with both pharmaceutical agents processed by microfluidic-assisted electrospinning. This strategy also leads to a longer delivery of the drugs at clinically relevant concentrations, along with a reduction of side effects. This proves that microfluidic-assisted electrospinning is a valid alternative to coaxial, for a controlled release of dual drugs to treat inflammatory arthritic diseases.

Supplementary data to this article can be found online at https://doi.org/10.1016/j.msec.2021.112585.

Declaration of competing interest

The authors confirm that there are no known conflicts of interest associated with this publication and there has been no significant financial support for this work that could have influenced its outcome.

Data availability

The raw/processed data required to reproduce these findings cannot be shared at this time as the data also forms part of an ongoing study.

References

[1] J.S. Smolen, D. Aletaha, I.B. McInnes, Rheumatoid arthritis, Lancet 388 (2016) 2023–2038, https://doi.org/10.1016/S0140-6736(16)30173-8.

[2] L.J. Crofford, Use of NSAIDs in treating patients with arthritis, Arthritis Res. Ther. 15 (2013), https://doi.org/10.1186/ar4174.

[3] C. Hua, F. Buttgereit, B. Combe, Glucocorticoids in rheumatoid arthritis: current status and future studies, RMD Open 6 (2020) 1–9, https://doi.org/10.1136/rmdopen-2017-000536.

[4] Q. Guo, Y. Wang, D. Xu, J. Nossent, N.J. Pavlos, J. Xu, Rheumatoid arthritis: pathological mechanisms and modern pharmacologic therapies, Bone Res. Rev. 6 (2018), https://doi.org/10.1038/s41413-018-0016-9.

[5] M.H. Schiff, P. Sadowski, Oral to subcutaneous methotrexate dose-conversion strategy in the treatment of rheumatoid arthritis, Rheumatol. Int. 37 (2017) 213–218, https://doi.org/10.1007/s00296-016-3621-1.

[6] E.Y. Kim, K.D. Moudgil, Immunomodulation of autoimmune arthritis by pro-inflammatory cytokines, Cytokine 98 (2017) 87–96, https://doi.org/10.1016/j.cyto.2017.04.012.

[7] M.A. Da Silva, A. Martins, A.A. Teixeira, R.L. Reis, N.M. Neves, Impact of biological agents and tissue engineering approaches on the treatment of rheumatic diseases, Tissue Eng. - Part B Rev. 16 (2010) 331–339, https://doi.org/10.1089/ten.teb.2009.0536.

[8] A. MaHam, Z. Tang, H. Wu, J. Wang, Y. Lin, Protein-based nanomedicine platforms for drug delivery, Small 5 (2009) 1706–1721, https://doi.org/10.1002/smll.200801602.

[9] G. Il Im, Perspective on intra-articular injection cell therapy for osteoarthritis treatment, Tissue Eng.Regen. Med. 16 (2019) 357–363, https://doi.org/10.1007/s13770-018-00176-6.

[10] N. Butoescu, O. Jordan, E. Doelker, Intra-articular drug delivery systems for the treatment of rheumatic diseases: a review of the factors influencing their performance, Eur. J. Pharm. Biopharm. 73 (2009) 205–218, https://doi.org/10.1016/j.ejpb.2009.06.009.

[11] E.R. Balmayor, K. Tuzlakoglu, H.S. Azevedo, R.L. Reis, Preparation and characterization of starch-poly-ε-caprolactone microparticles incorporating bioactive agents for drug delivery and tissue engineering applications, Acta Biomater. 5 (2009) 1035–1045, https://doi.org/10.1016/j.actbio.2008.11.006.

[12] E. Horisawa, T. Hirota, S. Kawazoe, J. Yamada, H. Yamamoto, H. Takeuchi, Y. Kawashima, Prolonged anti-inflammatory action of DL-lactide/glycolide copolymer nanospheres containing betamethasone sodium phosphate for an intra-articular delivery system in antigen-induced arthritic rabbit, Pharm. Res. 19 (2002) 403–410, https://doi.org/10.1023/A:1015123024113.

[13] S.Y. Ahn, C.H. Mun, S.H. Lee, Microfluidic spinning of fibrous alginate carrier having highly enhanced drug loading capability and delayed release profile, RSC Adv. 5 (2015) 15172–15181, https://doi.org/10.1039/c4ra11438h.

[14] Y. Sun, S. Cheng, W. Lu, Y. Wang, P. Zhang, Q. Yao, Electrospun fibers and their application in drug controlled release, biological dressings, tissue repair, and enzyme immobilization, RSC Adv. 9 (2019) 25712–25729, https://doi.org/10.1039/c9ra05012d.

[15] J.T. McCann, D. Li, Y. Xia, Electrospinning of nanofibers with core-sheath, hollow, or porous structures, J. Mater. Chem. 15 (2005) 735–738, https://doi.org/10.1039/b415094e.

[16] Y.Z. Zhang, X. Wang, Y. Feng, J. Li, C.T. Lim, S. Ramakrishna, Coaxial electrospinning of (fluorescein isothiocyanate-conjugated bovine serum albumin)-encapsulated poly(ε-caprolactone) nanofibers for sustained release, Biomacromolecules 7 (2006) 1049–1057, https://doi.org/10.1021/bm050743i.

[17] D.G. Yu, Y. Xu, Z. Li, L.P. Du, B.G. Zhao, X. Wang, Coaxial electrospinning with mixed solvents: from flat to round eudragit l100 nanofibers for better colon-targeted sustained drug release profiles, J. Nanomater. 2014 (2014), https://doi.org/10.1155/2014/967295.

[18] J. Wang, M. Windbergs, Controlled dual drug release by coaxial electrospun fibers – impact of the core fluid on drug encapsulation and release, Int. J. Pharm. 556 (2019) 363–371, https://doi.org/10.1016/j.ijpharm.2018.12.026.

[19] G. Cheng, C. Yin, H. Tu, S. Jiang, Q. Wang, X. Zhou, X. Xing, C. Xie, X. Shi, Y. Du, H. Deng, Z. Li, Controlled co-delivery of growth factors through layer-by-layer assembly of core shell nanofibers for improving bone regeneration, ACS Nano 13 (2019) 6372–6382, https://doi.org/10.1021/acsnano.8b06032.

[20] B. Pant, M. Park, S.J. Park, Drug delivery applications of core-sheath nanofibers prepared by coaxial electrospinning: a review, Pharmaceutics 11 (2019), https://doi.org/10.3390/pharmaceutics11070305.

[21] J. Cheng, Y. Jun, J. Qin, S.-H. Lee, Electrospinning versus microfluidic spinning of functional fibers for biomedical applications, Biomater. Rev. 114 (2017) 121–143, https://doi.org/10.1016/j.biomaterials.2016.10.040.

[22] I. Cimrák, M. Gusenbauer, T. Schrefl, Modelling and simulation of processes in microfluidic devices for biomedical applications, Comput. Math. Appl. 64 (2012) 278–288, https://doi.org/10.1016/j.camwa.2012.01.062.

[23] L. Zhang, Q. Chen, Y. Ma, J. Sun, Micro fluidic methods for fabrication and engineering of nanoparticle drug delivery systems, ACS Appl. Bio Mater. 3 (2020) 107–120, https://doi.org/10.1021/acsabm.9b00853.

[24] S. Sant, S.L. Tao, O.Z. Fisher, Q. Xu, N.A. Peppas, A. Khademhosseini, Microfabrication technologies for oral drug delivery, Adv. Drug Deliv. Rev. 64 (2012) 496–507, https://doi.org/10.1016/j.addr.2011.11.013.

[25] D.H. Reneker, Nanometre diameter fibres of polymer, produced by electrospinning, Nanotechnology 7 (1999) 216–223, https://doi.org/10.1088/0957-4484/7/3/009.

[26] E. Bacelo, M.A. Da Silva, C. Cunha, S. Faria, A. Carvalho, R.L. Reis, A. Martins, N. M. Neves, Biofunctional nanofibrous substrate for local TNF-capturing as a strategy to control inflammation in arthritic joints, Nanomaterials. 9 (2019) 1–16, https://doi.org/10.3390/nano9040567.

[27] A. Den Broeder, L.B.A. Van de Putte, R. Rau, M. Schattenkirchner, P.L.C.M. Van Riel, O. Sander, C. Binder, H. Fenner, Y. Bankmann, R. Velagapudi, J. Kempeni, H. Kupper, A single dose, placebo controlled study of the fully human anti-tumor necrosis factor-α antibody adalimumab (D2E7) in patients with rheumatoid arthritis, J. Rheumatol. 29 (2002) 2288–2298.

[28] M.L. Alves da Silva, A.R. Costa-pinto, A. Martins, V.M. Correlo, P. Sol, M. Bhattacharya, S. Faria, R.L. Reis, N.M. Neves, Conditioned medium as a strategy for human stem cells chondrogenic differentiation, J. Tissue Eng. Regen. Med. 12 (2013) 181–204.

[29] J.M. Kremer, D.A. Lawrence, R. Hamilton, I.B. McInnes, Long-term study of the impact of methotrexate on serum cytokines and lymphocyte subsets in patients with active rheumatoid arthritis: correlation with pharmacokinetic measures, RMD Open 2 (2016) 1–11, https://doi.org/10.1136/rmdopen-2016-000287.

[30] J. Bullock, S.A.A. Rizvi, A.M. Saleh, S.S. Ahmed, D.P. Do, R.A. Ansari, J. Ahmed, Rheumatoid arthritis: a brief overview of the treatment, Med. Princ. Pract. 27 (2019) 501–507, https://doi.org/10.1159/000493390.

[31] S.F. Ling, J. Bluett, Pharmacogenetics of methotrexate response in rheumatoid arthritis: an update, Pharmacogenomics 21 (2019) 3–6, https://doi.org/10.2217/pgs-2019-0154.

[32] R. Sanmartí, S. García-Rodríguez, J.M. Álvaro-Gracia, J.L. Andreu, A. Balsa, R. Cáliz, A. Fernández-Nebro, I. Ferraz-Amaro, J.J. Gómez-Reino, I. González-Álvaro, E. Martín-Mola, V.M. Martínez-Taboada, A.M. Ortiz, J. Tornero, S. Marsal, J.V. Moreno-Muelas, Update of the consensus statement of the Spanish Society of Rheumatology on the use of biological therapies in rheumatoid arthritis, Reumatol. Clin. 11 (2015) (2014) 279–294, https://doi.org/10.1016/j.reuma.2015.05.001.

[33] J.A. Singh, K.G. Saag, S.L. Bridges, E.A. Akl, R.R. Bannuru, M.C. Sullivan, E. Vaysbrot, C. McNaughton, M. Osani, R.H. Shmerling, J.R. Curtis, D.E. Furst, D. Parks, A. Kavanaugh, J. O'Dell, C. King, A. Leong, E.L. Matteson, J.T. Schousboe, B. Drevlow, S. Ginsberg, J. Grober, E.W. St.Clair, E. Tindall, A.S. Miller, T. McAlindon, American College of Rheumatology guideline for the treatment of rheumatoid arthritis, Arthritis Rheumatol. 68 (2016) 1–26, https://doi.org/10.1002/art.39480.

[34] Side effects and management of side effects of methotrexate in rheumatoid arthritis, Clin. Exp. Rheumatol. 28 (2010) S95–S101. https://www.clinexprheumatol.org/article.asp?a=4095%0Ahttp://ovidsp.ovid.com/ovidweb.cgi?T=JS&PAGE=reference&D=emed9&NEWS=N&AN=2010707610.

[35] M.A. Woodruff, D.W. Hutmacher, The return of a forgotten polymer - polycaprolactone in the 21st century, Prog. Polym. Sci. 35 (2010) 1217–1256, https://doi.org/10.1016/j.progpolymsci.2010.04.002.

[36] M.P. Arrieta, A.L. Gil, M. Yusef, J.M. Kenny, L. Peponi, Electrospinning of PCL-based blends: processing optimization for their scalable production, Materials (Basel). 13 (2020) 1–15, https://doi.org/10.3390/ma13173853.

[37] M. Krumova, D. López, R. Benavente, C. Mijangos, J.M. Pereña, Effect of crosslinking on the mechanical and thermal properties of poly(vinyl alcohol), Polymer (Guildf) 41 (2000) 9265–9272, https://doi.org/10.1016/S0032-3861(00)00287-1.

[38] F. Croisier, A.S. Duwez, C. Jérôme, A.F. Léonard, K.O. Van Der Werf, P.J. Dijkstra, M.L. Bennink, Mechanical testing of electrospun PCL fibers, Acta Biomater. 8 (2012) 218–224, https://doi.org/10.1016/j.actbio.2011.08.015.

[39] N.H.A. Ngadiman, M.Y. Noordin, D. Kurniawan, A. Idris, A.S.A. Shakir, Influence of polyvinyl alcohol molecular weight on the electrospun nanofiber mechanical properties, Procedia Manuf. 2 (2015) 568–572, https://doi.org/10.1016/j.promfg.2015.07.098.

[40] C.F. Guimarães, L. Gasperini, A.P. Marques, R.L. Reis, The stiffness of living tissues and its implications for tissue engineering, Nat. Rev. (2020), https://doi.org/10.1038/s41578-019-0169-1.

[41] D.L. Robinson, M.E. Kersh, N.C. Walsh, D.C. Ackland, R.N. de Steiger, M.G. Pandy, Mechanical properties of normal and osteoarthritic human articular cartilage, J. Mech. Behav. Biomed. Mater. 61 (2016) 96–109, https://doi.org/10.1016/j.jmbbm.2016.01.015.

[42] J.A.M. Wessels, T.W.J. Huizinga, H.J. Guchelaar, Recent insights in the pharmacological actions of methotrexate in the treatment of rheumatoid arthritis, Rheumatology 47 (2008) 249–255, https://doi.org/10.1093/rheumatology/kem279.

[43] A.H. Gerards, S. de Lathouder, E.R. de Groot, B.A.C. Dijkmans, L.A. Aarden, Inhibition of cytokine production by methotrexate.Studies in healthy volunteers and patients with rheumatoid arthritis, Rheumatology 42 (2003) 1189–1196, https://doi.org/10.1093/rheumatology/keg323.

[44] H. Lim, S.H. Lee, H.T. Lee, J.U. Lee, J.Y. Son, W. Shin, Y.S. Heo, Structural biology of the TNFα antagonists used in the treatment of rheumatoid arthritis, Int. J. Mol. Sci. 19 (2018) 1–14, https://doi.org/10.3390/ijms19030768.

[45] J. Širc, R. Hobzová, N. Kostina, M. Munzarová, M. Juklíčková, M. Lhotka, Š. Kubinová, A. Zajícová, J. Michálek, Morphological characterization of nanofibers: methods and application in practice, J. Nanomater. 2012 (2012), https://doi.org/10.1155/2012/327369.

[46] B. Dong, M.E. Smith, G.E. Wnek, Encapsulation of multiple biological compounds within a single electrospun fiber, Small 5 (2009) 1508–1512, https://doi.org/10.1002/smll.200801750.

[47] H. Jiang, Y. Hu, P. Zhao, Y. Li, K. Zhu, Modulation of protein release from biodegradable core – shell structured fibers prepared by coaxial electrospinning, J. Biomed. Mater. Res. B Appl. Biomater.2 (2006) 50–57, https://doi.org/10.1002/jbmb.

[48] Y. Lee, F. Mei, M. Bai, S. Zhao, D. Chen, Release pro file characteristics of biodegradable-polymer-coated drug particles fabricated by dual-capillary electrospray, J. Control. Release 145 (2010) 58–65, https://doi.org/10.1016/j.jconrel.2010.03.014.

[49] W. Chanput, J.J. Mes, H.J. Wichers, THP-1 cell line: an in vitro cell model for immune modulation approach, Int. Immunopharmacol. 23 (2014) 37–45, https://doi.org/10.1016/j.intimp.2014.08.002.

[50] S. Pirmardvand Chegini, J. Varshosaz, S. Taymouri, Recent approaches for targeted drug delivery in rheumatoid arthritis diagnosis and treatment, Artif. Cells Nanomed. Biotechnol. 46 (2018) 502–514, https://doi.org/10.1080/21691401.2018.1460373.